GRADUATE AERONAUTICAL LABORATORIES
CALIFORNIA INSTITUTE OF TECHNOLOGY

Hydroacoustic Testing of a NACA–66 (MOD) Hydrofoil in the GALCIT High Speed Water Tunnel

Paul E. Dimotakis

GALCIT HSWT Report 1143
4 March 1991

Firestone Flight Sciences Laboratory

Guggenheim Aeronautical Laboratory

Karman Laboratory of Fluid Mechanics and Jet Propulsion

Pasadena

GRADUATE AERONAUTICAL LABORATORIES
CALIFORNIA INSTITUTE of TECHNOLOGY
Pasadena, California 91125

Hydroacoustic Testing of a NACA–66 (MOD) Hydrofoil in the GALCIT High Speed Water Tunnel

Paul E. Dimotakis

Final Report

Contract Nos. N00167–89–M–6245 and N00167–90–M–0348

GALCIT HSWT Report 1143

4 March 1991

Table of Contents

1. Introduction

The work described in this report represents a primarily exploratory effort to assess the feasibility of performing accurate hydroacoustic measurements at high signal-to-noise ratios, in the GALCIT High Speed Water Tunnel (HSWT), hereafter referred to as the Tunnel, to characterize the hydroacoustic environment in the HSWT 2-D test section, and to complement the force and flow visualization measurements that were performed using the two-dimensional, NACA 66 (MOD) hydrofoil in the recent past. See Baloga (1982), Dimotakis *et al.* (1988), Shen & Dimotakis 1989a, and Shen & Dimotakis 1989b. This work was also a sequel to earlier hydroacoustic measurements that were performed by S. Barker (1974, 1975, 1976) in the same facility.

The development effort was begun in 1989 with the tests reported here performed during July 1990. These were designed and conducted by the author, in collaboration with

a. Dr. Young T. Shen, of the David Taylor Naval Research Center,

with the assistance of the GALCIT team comprised by

b. Dr. Daniel B. Lang, who was primarily responsible for the design of the analog signal and digital data acquisition system,

c. Mr. Herbert Gaebler, with the assistance of Mr. Pavel Svitek and Mr. Harry Hamaguchi, as Test Operators.

Finally,

d. The photographic data were recorded by Mr. Harry Hamaguchi with the assistance of Mr. Alan Goudey, who was responsible for the modifications and maintenance of the high voltage photographic flash electronic equipment.

The tests described in this report were supported by the Navy Contract No. N00167–90–M–0348. The preceding development effort and first feasibility study, as well as the Tunnel modifications that were necessary for these tests to be conducted, were supported by Navy Contract No. N00167–89–M–6245.

2. Test setup

The NACA 66 (MOD) hydrofoil was mounted in the Tunnel 2-D test section force balance, as was documented in Baloga (1982) and in Dimotakis *et al.* (1989). As no force measurements were required for these tests, the gap between the hydrofoil tip and the window test section sidewall was filled by cementing a thin neoprene gasket, cut to conform to the hydrofoil thickness profile. In earlier exploratory tests, it had been established that leaving the gap open resulted in early cavitation in the gap. The intent in this work was to study the hydroacoustic field from the two-dimensional flow and cavitation, to the extent feasible.

2.1 Acoustic transducer assemblies

The hydroacoustic receiver and driver (projector) were supplied by DTRC. The receiver was a small diameter (external $\phi = 0.25''$), high frequency hydrophone. The driver was a larger (external $\phi = 1.125''$), lower frequency response hydrophone. The spectral sensitivity response for these transducers is included as Appendix A. It was adequately flat, for the purposes of this test, that it was decided that no separate compensation of the measured hydroacoustic spectra was necessary. The second reason was that the calibrated response that was supplied by the Navy was measured in a free field acoustic test. The response of the receiver and driver, in their respective assemblies (see below), could be expected to be different and would required a separate calibration.

Given that the acoustic driver transducer was characterized by a very nearly uniform sensitivity, in the frequency range from 100 Hz to 100 kHz (Appendix A, p. 49), it was decided that the white noise excitation calibration that was performed to measure the acoustic admittance of the Tunnel (plus transducers) also served the purpose of spectral sensitivity compensation.

The receiver and driver were each mounted in custom-designed assemblies, comprised of a cone of nominally 20° half-angle, terminated with a $0.3''$ layer of acoustically impedance-matched "rho-c rubber" material*. The diameter of the rho-c rubber flared end was $\sim 5''$.

For the hydroacoustic measurements, the interior of the cone was always full of water, with provisions for maintaining the internal pressure close to that of the test section and for flushing the inevitable air bubbles that came out of solution and collected in the course of the tests, especially at the lowest static pressures. This design proved very successful, as

---

* Goodrich, castable rho-c, 60 durometer acoustic material #35065 (Part A & B).

a. the transducer assemblies had no internal resonances of their own,

b. they permitted the receiver and driver to be flush with the (flat) test section upper and lower guidewalls, respectively,

c. the 5″ diameter allowed for the Tunnel wall turbulent boundary layer (pressure fluctuation) noise to be averaged over its area, making the receiver much more selective to "far field" acoustic noise emanating from the hydrofoil,

and

d. provided for some "antenna gain" for frequencies corresponding to wavelengths that were comparable or smaller than the exit diameter of 5″ of the flared cone.

The hydroacoustic receiver and driver assemblies were, in turn, mounted flush in the top and bottom test section flow guidewalls. See Tunnel test section schematic in Fig. 1.

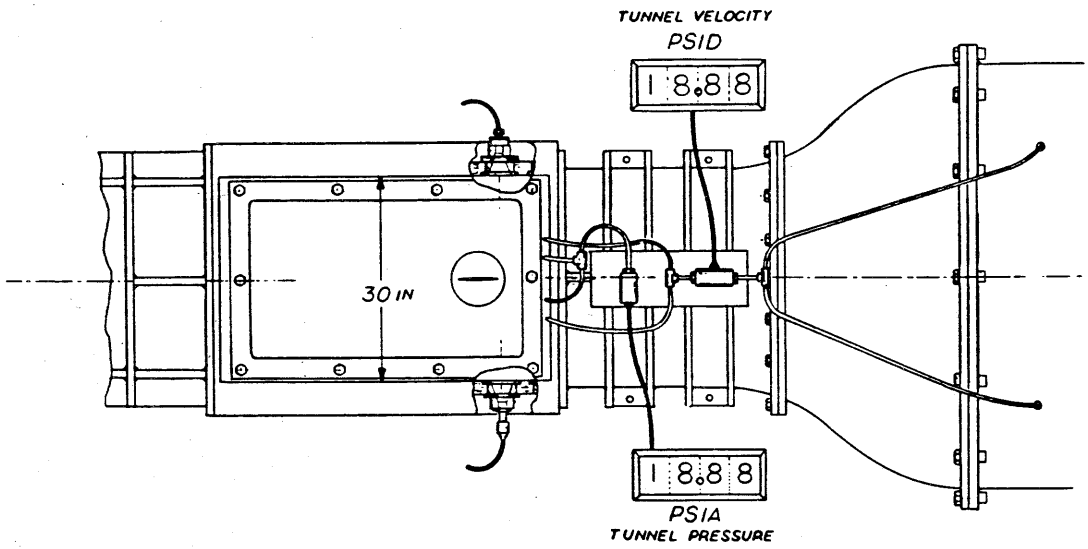

FIG. 1 Two-dimensional test section layout. Receiving hydrophone mounted on top. Acoustic driver mounted on the bottom. Line of sight of the two acoustic transducers just ahead of hydrofoil leading edge (flow from right to left).

2.2 Signal/data acquisition and processing

The receiver cable was shortened to $\sim 9''$ and additional shielding was provided to minimize electronic noise pick-up*. The resulting signal was amplified by a Stanford Research SR–560 low-noise amplifier/band-filter combination. Its output signal was additionally buffered at the input of the A/D converter** and converted to digital form by a 12-bit, 200 kHz, Data Translation Model 3362 A/D converter. The data were recorded on a custom-developed, DEC-11/73 CPU-based data acquisition system, running the DEC RT-11 real time operating system. They were subsequently transferred, *via* ethernet, to a micro-VAX cluster system, under VMS, for subsequent processing.

The data acquisition system has been developed by Dr. Dan Lang, in collaboration with the author, over the last 10 years, or so. The spectral and other data analysis software were developed by the author over the years. That software still represents work in progress. Its documentation is beyond the purposes of this report.

---

* At least in the laboratory environment in which these tests were conducted, the original cable that was provided with the transducers was found to be responsible for a measurable noise contribution.

** By a custom-designed unity gain amplifier designed by Dr. Dan Lang.

3. Test sequence

The first few runs (17 July 1990) were exploratory. Their purpose was to measure background levels, equipment and instrumentation performance, as well as check the data acquisition and processing software. These will be described below.

3.1 17 July 1990: 90-1

The first set of runs were recorded with the hydrofoil set at an angle of attack of $\alpha = -0.3°$, closely corresponding to zero lift. This was done in an effort to investigate fully wetted flow so as to isolate hydroacoustic energy emanating from cavitation, as opposed to hydroacoustic excitation emanating from turbulent boundary layers in the tunnel, tunnel machinery vibration, tunnel walls acoustic excitation and emission, *etc.*

The summary log `YTSlog.0190` for these first exploratory runs is listed below. The Tunnel water air content (top right in the log listing) was measured using a Van Slyke apparatus.

```
YTSlog.0190     17-Jul-90               Bearing oil pump + A/C on.
                10:32 am                Air = 11.6 ml/l.
                10:50 am                Air = 11.8 ml/l.
-------------------------------------------------------------------------------
Run    alpha   P/psia  U/(ft/s) Gain    Comments
-------------------------------------------------------------------------------
500    -0.3    16.58     off    1000    10Hz-100kHz BW.  200kHz clock.
501    -0.3    16.46     7rpm   1000
502    -0.3    16.19     9.41   1000
503    -0.3    16.66    21.14   1000
504    -0.3    16.86    30.34   1000
505    -0.3    16.23    37.01    500
506    -0.3    18.39     off     500
507    -0.3    18.05    49.79    500    A few points out of A/D bounds
508    -0.3    20.39    39.84    500
509    -0.3    14.85    39.95    500
510    -0.3     9.87    39.96    500
511    -0.3     7.36    39.83    500
512    -0.3     6.02    40.11    500
513    -0.3     4.98    39.92    500
-------------------------------------------------------------------------------
```

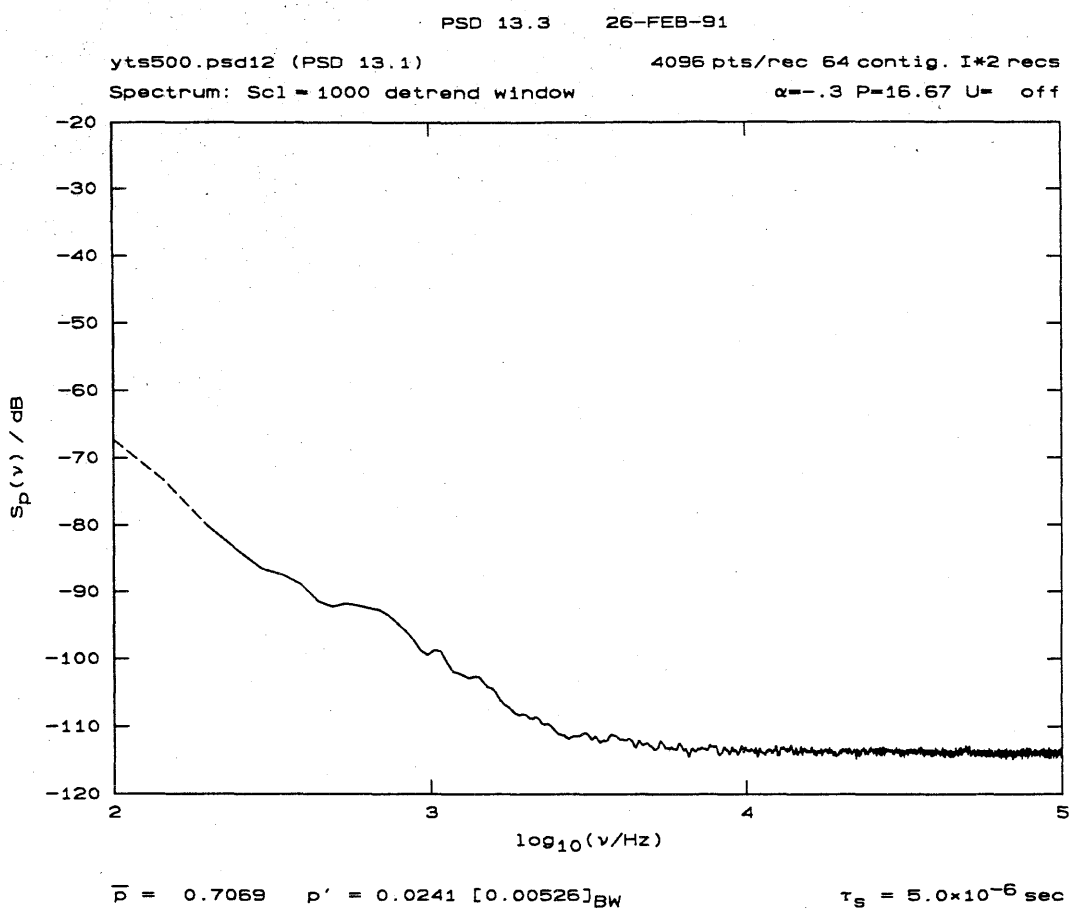

FIG. 2 Run 500, background noise hydroacoustic power spectrum.

The power spectrum for the background and electronic noise (amplifier gain of 1000) for Run 500 is plotted in Fig. 2. This can be compared to the power spectrum for Run 501 with the tunnel motor just barely on (7 rpm), which is plotted in Fig. 3.

These spectra were computed from the pressure transducer output signal, which was amplified by a Stanford Research Systems SR-560 low-noise signal amplifier, at a gain of 1000, as noted in the log, and a band-pass filter set from 10 Hz to 100 kHz.

For the purposes of computing these acoustic power spectra, the data were treated as comprised of 64 contiguous records, of 4096 12-bit A/D output data points per record, as labeled at the top right of these plots. The sampling period between data points is labeled at the bottom right and, as indicated for these data, was 5 μs, corresponding to an A/D sampling frequency of 200 kHz, consistent with the low-pass filter setting of 100 kHz *vis-à-vis* the Nyquist sampling criterion.

As can be seen in the spectrum in Fig. 3, even though the flow is virtually at rest, there is considerable hydroacoustic excitation in the 1 kHz to 10 kHz fre-

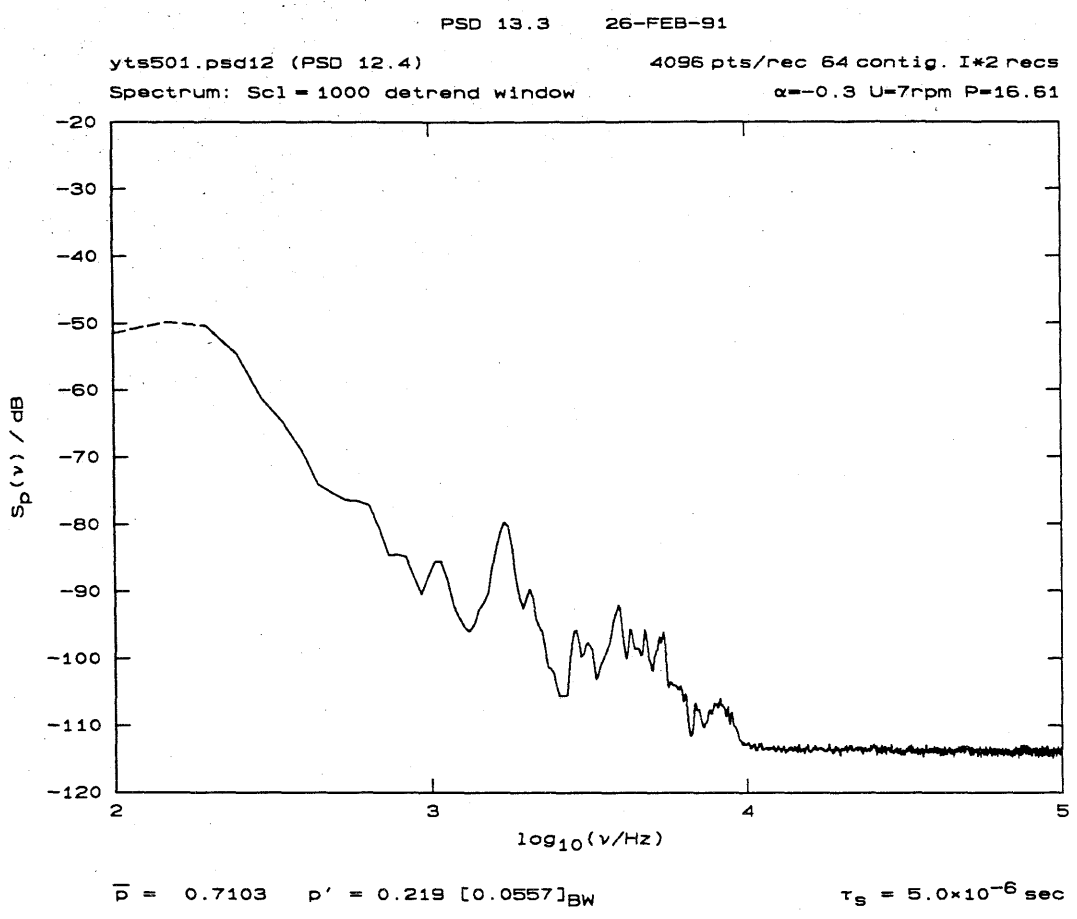

FIG. 3 Run 501 (Tunnel motor on at 7 rpm) hydroacoustic power spectrum.

quency range*. This source of noise was subsequently traced to some of the Tunnel machinery, as will be discussed below.

The spectra in Figs. 2 and 3 can be compared to the spectrum of the Run 503 hydroacoustic data, plotted in Fig. 4, at a Tunnel speed of $U_{\text{test}} = 30.34\,\text{ft/s}$ and a Tunnel test section pressure of $p_{\text{test}} = 16.86\,\text{psia}$.

The very large dynamic range (signal-to-noise ratio) of these spectra should be noted. It represents the highest of any hydroacoustic spectra recorded for such a flow in a test facility, that we are aware of. For some of the data to be presented later, the dynamic range is as high as $90-95\,\text{dB}$**. This dynamic range may appear difficult to reconcile with the 12-bit dynamic range of the analog-to-digital (A/D) converters that were employed to acquire the digital data. It was achieved using

---

* Figs. 2 and 3 have been aligned on the respective pages so that they can be easily compared by holding the two pages against the light.

** Defined here as the ratio (dB difference) of the highest power spectrum value to the noise level.

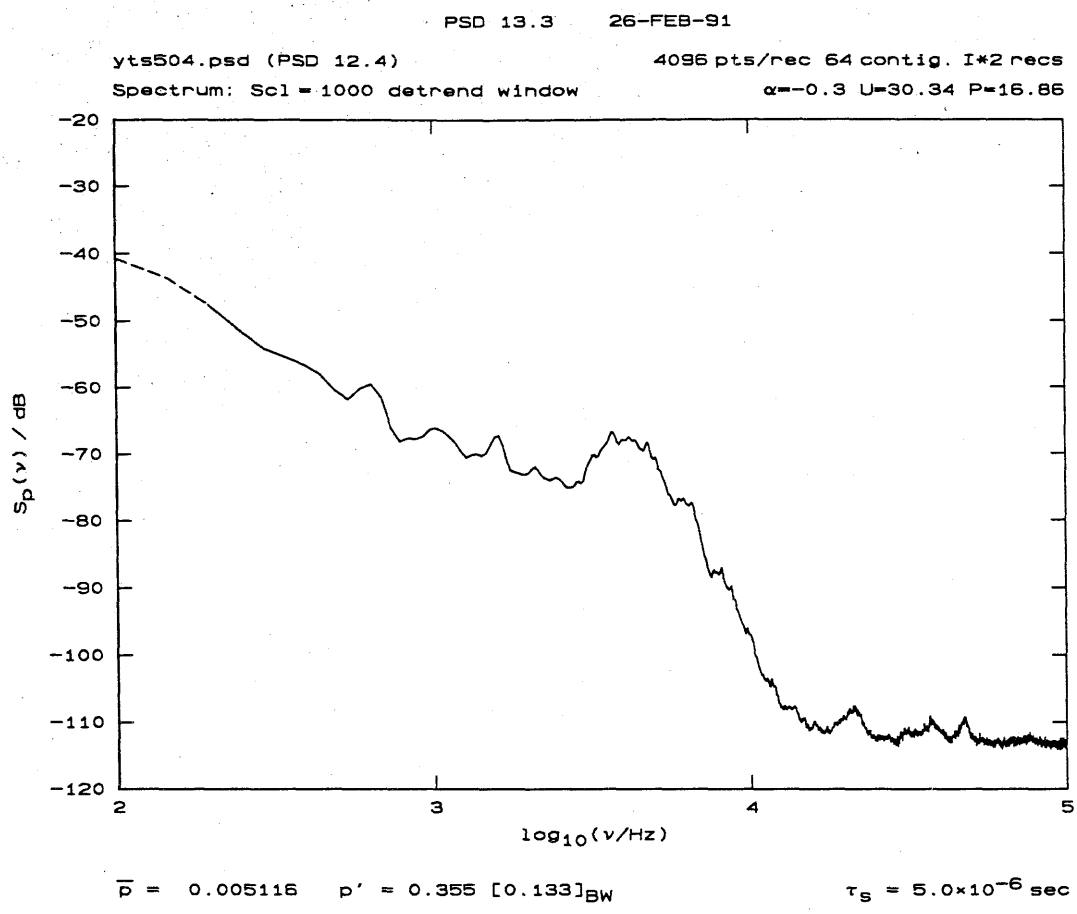

FIG. 4 Run 504 hydroacoustic power spectrum, recorded at a Tunnel speed and pressure of $U_{\text{test}} = 30.34\,\text{ft/s}$ and $p_{\text{test}} = 16.86\,\text{psia}$, respectively.

a host of signal acquisition and processing techniques that have been developed in our laboratory over the last ten years, or so.

To the extent that the acoustic spectrum in Fig. 4 can be regarded as the superposition of the background, plus Tunnel machinery, noise and the flow noise at $U_{\text{test}} = 30.34\,\text{ft/s}$, we can estimate the latter by subtracting the background spectrum, with the Tunnel motor on (Fig. 3). The resulting spectrum is plotted in Fig. 5.

As can be ascertained by comparing Figs. 4 and 5 the background noise represents a negligible contribution for frequencies below 10 kHz, or so, at these flow conditions. This is true even including the Tunnel motor bearing oil pump noise; a noise source we were subsequently able to eliminate.

The peaks at frequencies in excess of 10 kHz are the result of the non-uniform acoustic admittance of the Tunnel, as will be shown below. They represent a near-resonant excitation by flow-generated acoustic power of various acoustic modes in

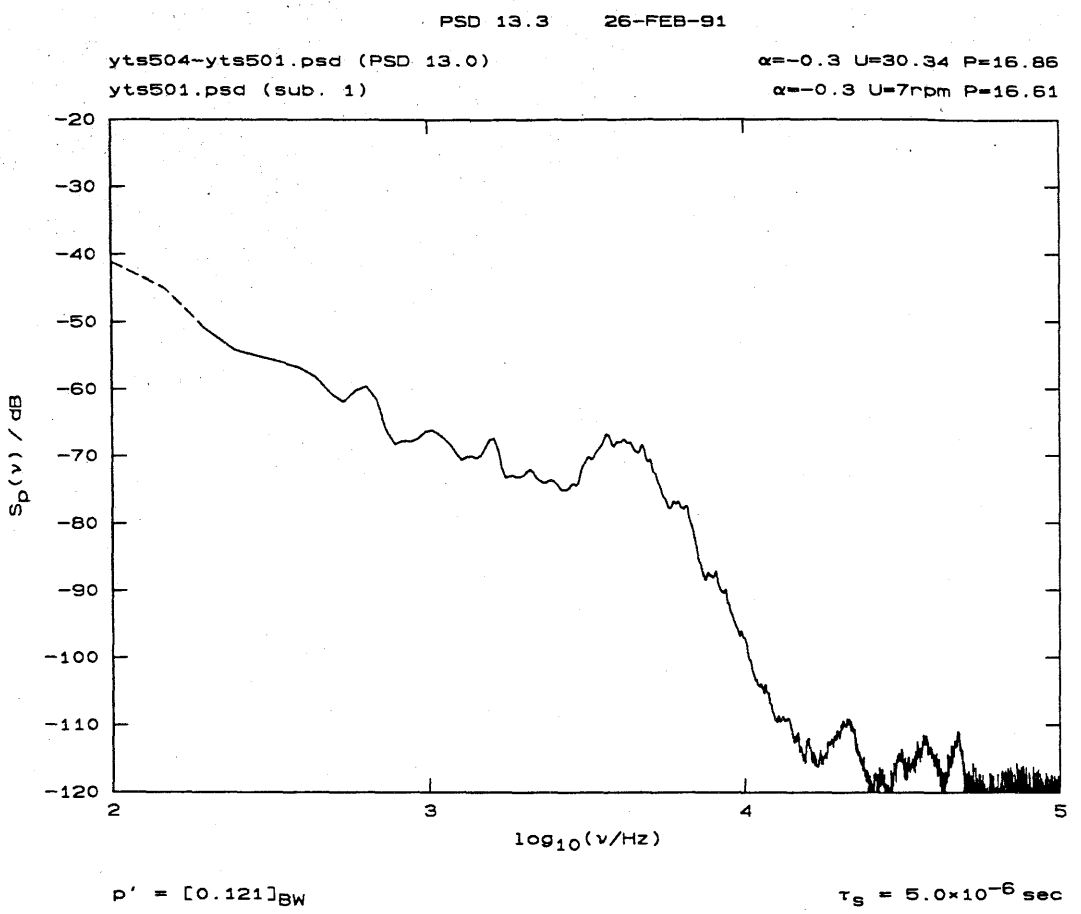

FIG. 5 Run 504 hydroacoustic power spectrum, recorded at a Tunnel speed and pressure of $U_{\text{test}} = 30.34\,\text{ft/s}$ and $p_{\text{test}} = 16.86\,\text{psia}$, respectively, with the background noise (Fig. 3) subtracted.

the High Speed Water Tunnel. They indicate that even at frequencies as high as can be seen in these spectra, there is flow-generated acoustic energy. They are absent in the acoustic spectra in Figs. 2 and 3, which were recorded with the flow at a fraction of a foot per second.

It would require a much more highly acoustically damped Tunnel, with near anechoic properties at these frequencies, to eliminate these resonances. These were observed as part of this test for the first time and would typically not be observable, were it not for the very high signal-to-noise ratio in these measurements. It is noted here that while a truly anechoic environment would be difficult to engineer as an afterthought in a facility such as this, one can nevertheless expect to realize considerable benefits from applying such measures even after the fact.

The acoustic signal at a higher test section velocity of $U_{\text{test}} = 37.01\,\text{ft/s}$ saturated the amplifier at a gain of 1000. Accordingly, the amplifier gain was lowered

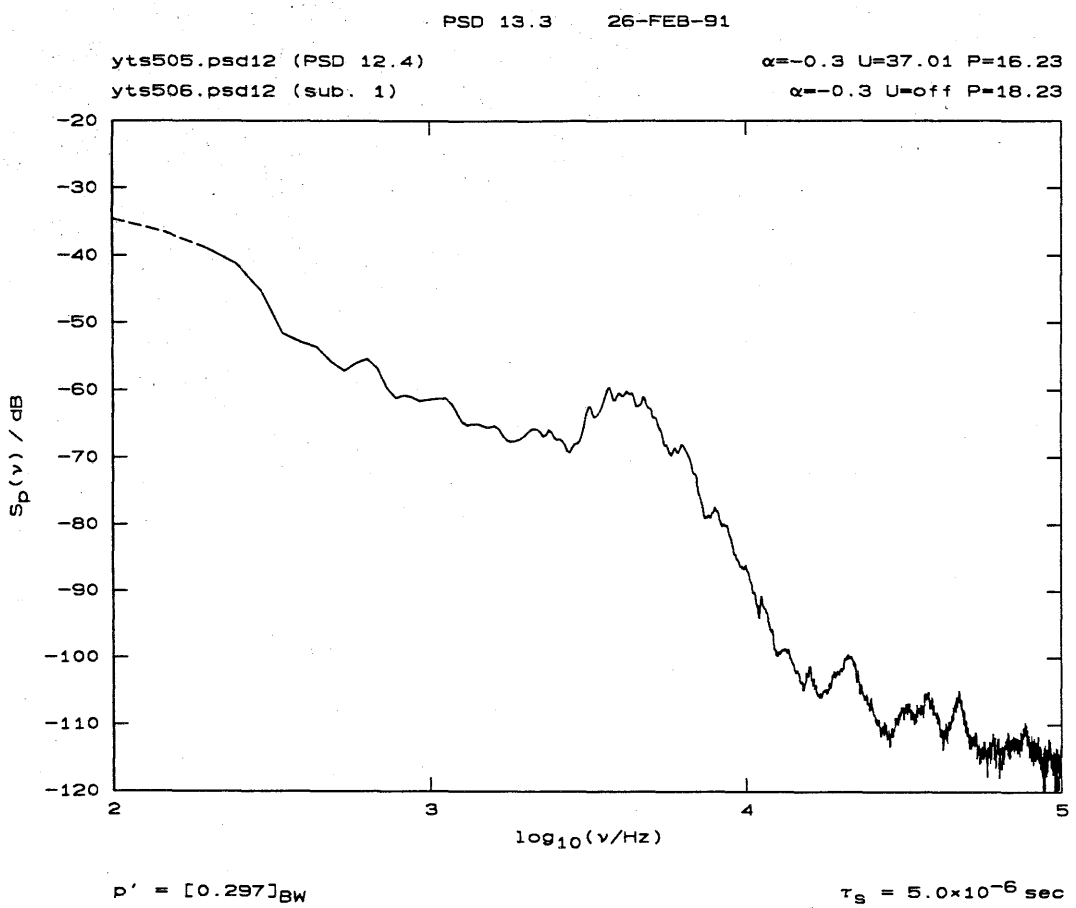

FIG. 6 Run 506 hydroacoustic power spectrum, recorded at a Tunnel speed and pressure of $U_{\text{test}} = 37.01\,\text{ft/s}$ and $p_{\text{test}} = 16.23\,\text{psia}$, respectively, with the background noise (Run 506) subtracted.

to 500, as indicated, and the data were recorded at this setting (Run 505). This required the electronic and other background to be recorded anew at this gain setting (Run 506; Tunnel motor off). The spectrum for this flow condition, with the noise as measured in Run 506 subtracted, is plotted in Fig. 6. As can be seen, at the higher velocity, the spectrum now registers acoustic power at frequencies above 10 kHz, extending to 100 kHz. This should be contrasted to the spectrum recorded at $U_{\text{test}} = 30.34\,\text{ft/s}$ (*cf.* Fig. 5). Again, it is noted that were it not for the very high signal-to-noise ratio in these measurements, the increase in acoustic power at these frequencies would not be discernible.

Finally, a scan with respect to test section pressure (cavitation number) was made, holding the Tunnel speed constant at $U_{\text{test}} \simeq 40\,\text{ft/s}$. The resulting spectra are plotted in Fig. 7, each offset by 10 dB, to facilitate the comparison. At these Tunnel speeds, the background noise spectrum represents a negligible contribution (*cf.* Fig. 6) and was not subtracted from the flow spectra.

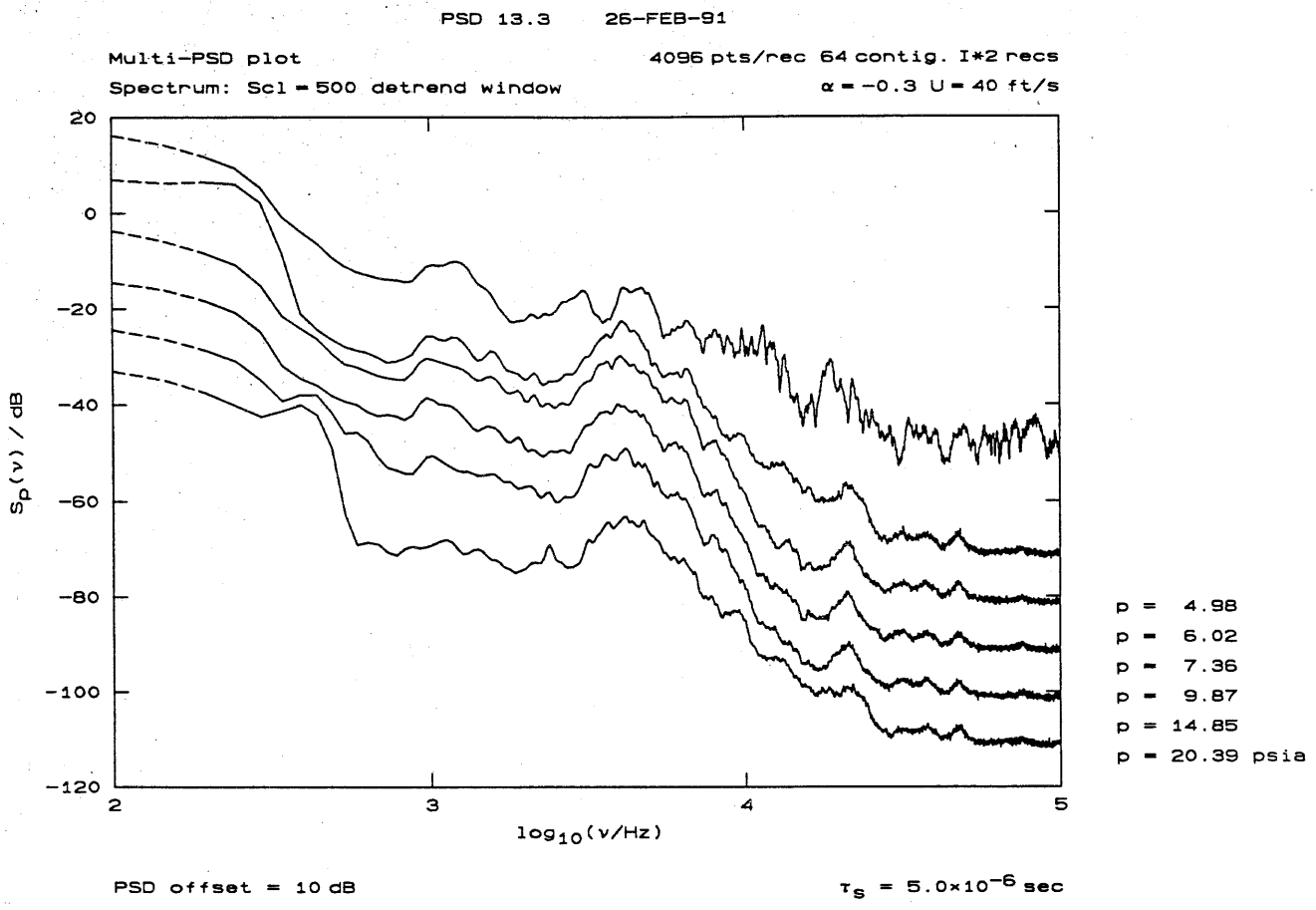

FIG. 7 Hydroacoustic power spectra, recorded at a Tunnel speed of $U_{\text{test}} \simeq 40\,\text{ft/s}$ for variable Tunnel pressure (as indicated, legend right). Bottom spectrum plotted with its origin as indicated. Spectra above each offset by 10 dB.

As can be seen, the hydroacoustic spectra indicate a qualitative departure in behavior at the lowest pressure. While no specific investigation was undertaken in this sequence to establish the reason for this, subsequent data suggest that this is attributable to *cavitation initiated at the hydrofoil root*, *i.e.* the junction between the hydrofoil and the fairing plate, as well as the hydrofoil tip†. At these locations, the flow can be expected to realize the lowest static pressure; a result of the horseshoe vortex that must be wrapped around the hydrofoil leading edge.

† The gap between the hydrofoil and the test section window at the hydrofoil tip was closed using a thin cemented layer of neoprene sheet. This was cut flush with the hydrofoil thickness profile. The test section window flexure with test section pressure was minimized by using an external stiffening support applied to the middle of the test section window. Window flexure was monitored with a dial indicator opposite the hydrofoil mid-chord point.

3.2 17 July 1990: 90-2

For the next test sequence, the hydrofoil was set at an angle of attack of $\alpha = 4°$ and the Tunnel speed was held at $U_{\text{test}} \simeq 28.6\,\text{ft/s}$. The summary log for this sequence is listed below.

YTSlog.0290 17-Jul-90 Air = 11.6, 11.8 ml/l.

Run	alpha	P/psia	U/(ft/s)	Gain	Comments
514	4.0	19.92	28.64	500	
515	4.0	14.99	28.69	500	
516	4.0	12.40	28.78	500	
517	4.0	13.64	28.63	500	
518	4.0	9.95	28.59	500	Cav. inception (root)
519	4.0	9.01	28.58	500	
520	4.0	7.97	28.51	500	
521	4.0	6.97	28.61	500	Transient LE cavitation
522	4.0	6.00	28.65	500	Lc=1.25"
523	4.0	5.55	28.44	500	Lc=2.5"
524	4.0	5.11	28.59	500	Lc=4.0"
525	4.0	4.96	28.48	500	3.75<Lc<-4.25"
526	4.0	4.83	28.48	500	Buffetting to TE

Note that cavitation inception, as determined using stroboscopic light illumination, was detected at a test section pressure of $p_{\text{test}} \simeq 10\,\text{psia}$. The spectra for this sequence are plotted in Fig. 8, each offset by 10 dB. Again, the (small) background noise was not subtracted.

It is significant that the hydroacoustic spectrum, at a test section pressure of $p_{\text{test}} = 13.64\,\text{psia}$ (third from the bottom) is characterized by substantial high frequency ($10\,\text{kHz} \leq \text{f} \leq 100\,\text{kHz}$) content that marks cavitation discernible by visual means at the lower pressures. When it could first be detected stroboscopically ($p_{\text{test}} \simeq 10\,\text{psia}$), this cavitation could be seen to occur at the hydrofoil root, just above the hydrofoil leading edge. As noted earlier, this region in the flow can be expected to produce the lowest static pressures, *and is also associated with a relatively long residence time for travelling nucleation bubbles*, with fluid particle trajectories passing close to the leading edge stagnation region.

Note also that the spectrum at $p_{\text{test}} = 9.95\,\text{psia}$ (Run 518), corresponding to the visual indication of cavitation inception, *does* exhibit a larger increase in acoustic power. Indeed, an increase extending to frequencies down to 1 kHz.

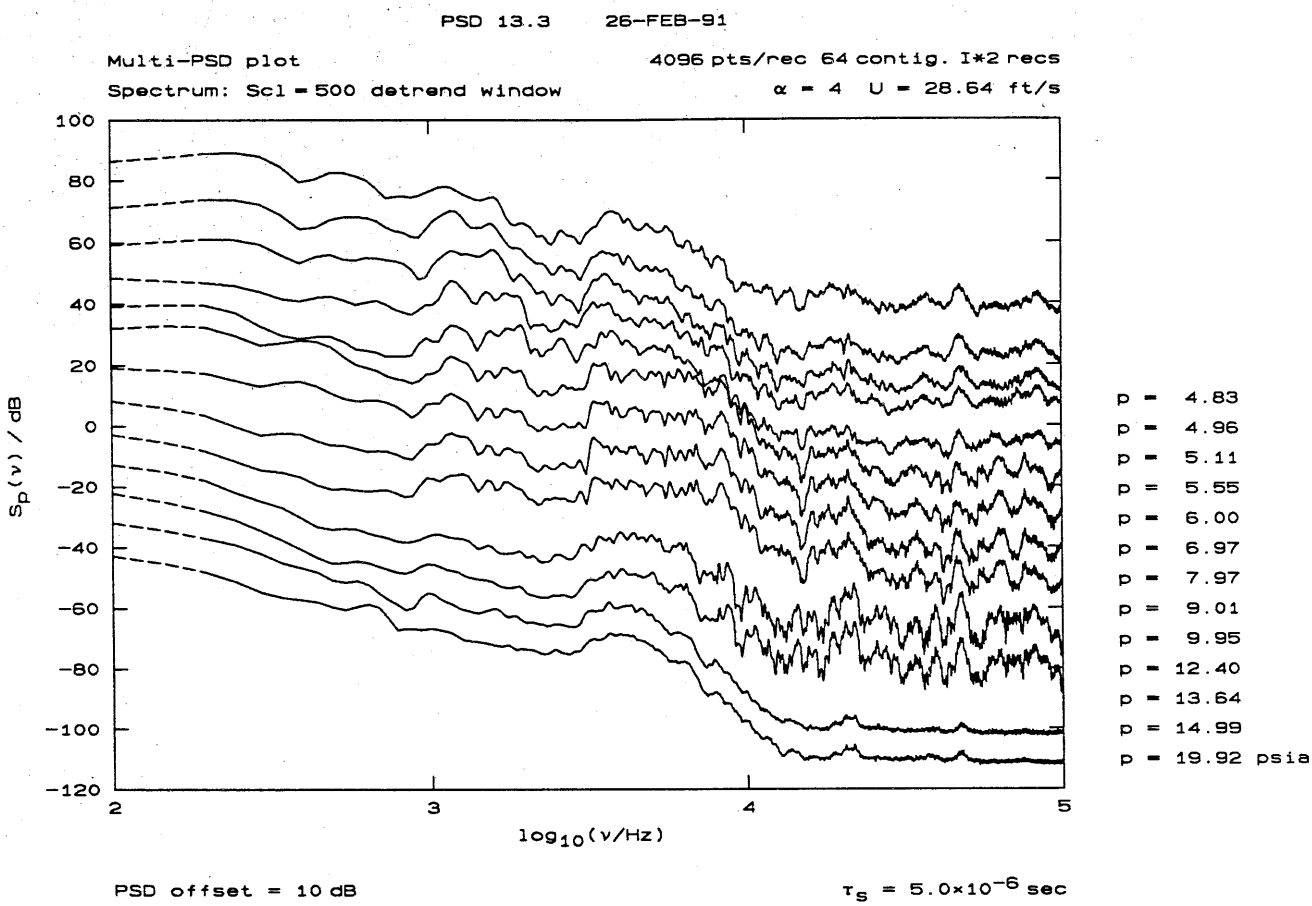

FIG. 8 Hydroacoustic power spectra. Tunnel speed of $U_{\text{test}} \simeq 28.6\,\text{ft/s}$. Variable Tunnel pressure (as indicated, legend right). Bottom spectrum plotted with its origin as indicated. Spectra offset by 10 dB.

Sighting along the spectrum axis of these spectra, it can be seen that the prominent frequency features are independent of the test section pressure, even down to pressure values corresponding to rather low test section cavitation numbers. This suggests that the speed of sound is not significantly affected as the pressure is lowered. This may be considered as a surprising result, especially as it is claimed to hold down to test section pressures that could be regarded as potentially resulting in gas bubbles coming out of solution. The speed of sound being very sensitive to bubble void fraction, it is, in turn, a very sensitive indicator of such changes. That no such changes can be seen with test section pressure can be credited to the long residence time of the recirculating flow and high pressure in the Tunnel resorber at these flow velocities.

An independent investigation was undertaken to confirm this finding, using the acoustic transmitter located on the bottom test section guidewall. Using phase-sensitive detection techniques and a transmitter frequency of 120 kHz, it was found

that the speed of sound was constant to one part in 50,000, or better, at this Tunnel speed, through the range in test section pressure (4.83 psia $\leq p_{\text{test}} \leq$ 29.92 psia) in the pressure scan sequence in `YTSlog.0290`.

3.3 19 July 1990: 90-3

It was decided to remove the hydrofoil to add a fillet at the junction formed with the fairing section. It was hoped that this would minimize the strength of the root vortex, minimizing the reduction in the pressure in its core. The Tunnel was refilled and deaerated. The hydrofoil angle of attack was left at $\alpha = 4°$. The log file for these runs is listed below.

```
YTSlog.0390     19-Jul-90              Filletted foil.
                                       Air = 12.5, 12.6 ml/l.
-------------------------------------------------------------------------------
Run    alpha   P/psia  U/(ft/s) Gain    Comments
-------------------------------------------------------------------------------
527     4.0     19.79     off    500    Vacuum pump + filter pumps on.
528     4.0     19.56     off    500    Vacuum pump + filter pumps off.
529     4.0     19.90    7rpm    500
530     4.0     19.17   30.14     500
531     4.0     14.89   30.26     500
532     4.0      9.64   28.51     500
533     4.0      8.00   34.56     500    Root cavitation.        215 rpm.
534     4.0     24.82   34.62     500
535     4.0     14.75   34.53     500    Root cavitation.
536     4.0     12.45   34.59     500
537     4.0      9.90   34.54     500
538     4.0     10.01   34.50     200
539     4.0      8.11   34.41     200
540     4.0      7.97   34.50     200    3" LE cavity
541     4.0      7.00   34.36     200    4" LE cavity
542     4.0      6.75   34.11     200    Buffetting.  A/D saturation.
543     4.0      6.73   34.72      50    BW = 0.3Hz-3kHz.  Clock =  10kHz.
544     4.0     16.29    7rpm     200    BW = 10Hz-100kHz. Clock = 200kHz.
545     4.0     16.25    7rpm      50
-------------------------------------------------------------------------------
```

No significant differences were noted in the spectra between this sequence and the data in `YTSlog.0290`, listed on p. 12 (*cf.* spectra in Fig. 8).

A separate study was undertaken of the low frequency part of the pressure fluctuation spectrum, at a test section pressure where the flow results in buffetting ($p_{\text{test}} \simeq 6.73 - 6.75\,\text{psia}$). It could be determined by direct observation that the buffetting frequency was quite regular, estimated visually at about 1 Hz. To investigate this frequency regime, the amplifier band-pass filter was set from 0.3 Hz to 3 kHz, with the A/D sampling frequency at 10 kHz. For this run, the data were processed as comprised of fewer, longer ($2^{14} = 16\,384$ point) records, resulting in a larger frequency range. The resulting spectrum is plotted in Fig. 9.

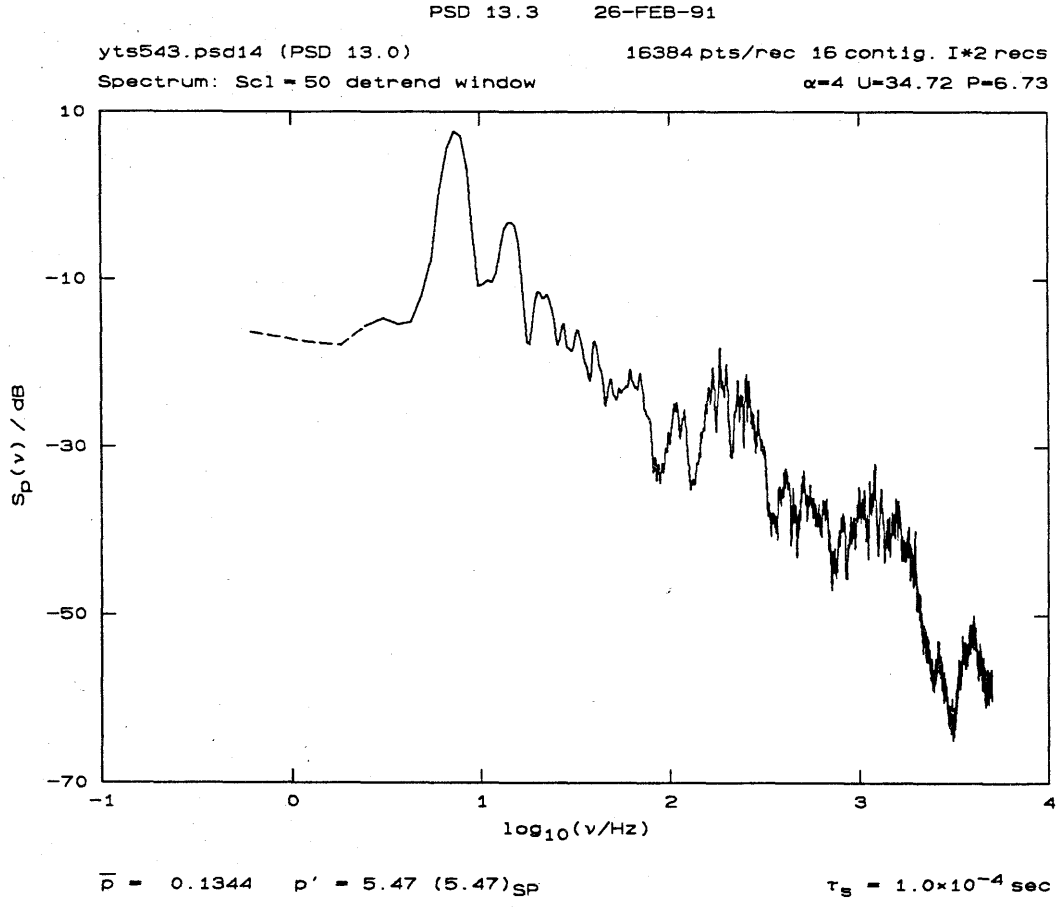

FIG. 9 Pressure fluctuation spectrum at buffetting conditions (Run 543). Tunnel speed: $U_{\text{test}} = 34.72\,\text{ft/s}$. Tunnel pressure: $p_{\text{test}} = 6.73\,\text{psia}$. A/D sampling frequency: $f_s = 10\,\text{kHz}$.

The very large peak at a frequency just below 1 Hz is conspicuous. The associated pressure fluctuations at this frequency should not be regarded as acoustic, however. They can best be described as hydrodynamic, arising from the time-dependent test section blockage due to the unstable, oscillating cavitation bubble that extends well beyond the hydrofoil trailing edge, *via* the Bernoulli equation.

3.4 20 July 1990: 90-4

To investigate the resonant frequency behavior at high frequencies, *i.e.* at $f >$ 10 kHz, an effort to measure the Tunnel acoustic *admittance* was made, using the acoustic exciter (projector) mounted at the bottom test section guidewall. This was driven by a custom-designed white noise generator*. This produced an excitation spectrum which was measured to be flat to within ± 1 dB in the frequency range from 100 Hz to 100 kHz.

A second issue that was addressed concerned the acoustic power in the vicinity of 4 kHz, which seems to be excited by the flow, or Tunnel machinery. As can be seen by comparing the spectra in Fig. 7, at $U_{\text{test}} \simeq 40$ ft/s, and in Fig. 8 at $U_{\text{test}} \simeq 28.6$ ft/s, however, this excitation (around 4 kHz) appears to be independent of Tunnel speed. It was decided to attempt to see if it could be traced to some extraneous source. The resulting data run log `YTSlog.0490` is listed below.

`YTSlog.0490  20-Jul-90  Air = 12.1, 12.3 ml/l.`

Run	alpha	P/psia	U/(ft/s)	Gain	Comments
546	4.0	17.46	off	500	Noise generator off
547	4.0	17.17	off	500	Noise generator @1.09 Vrms
548	4.0	17.06	7rpm	500	Noise generator off
549	4.0	17.01	7rpm	500	Noise generator @1.09 Vrms
					Noise ~4kHz traced to bearing oil pump
550	4.0	17.72	7rpm	500	Bearing pump off.
551	-0.3	19.98	19.95	500	124 rpm
552	-0.3	16.75	29.34	500	181 rpm
553	-0.3	16.47	34.23	500	212 rpm
554	-0.3	16.84	39.57	500	243 rpm
555	-0.3	20.06	44.16	500	272 rpm

Figure 10 is a plot of the acoustic spectrum detected with no flow (Run 547: Tunnel motor off), with the acoustic transmitter (projector) driven with the white noise generator at an amplitude of 1.09 V rms. The background noise spectrum, as estimated from the data in Run 546, has been subtracted. As can be seen in this spectrum, the Tunnel can be described as possessing a fairly flat acoustic admittance (response), *for acoustic paths across the test section height*, for frequencies below 10 kHz. On the other hand, it is also characterized by resonances with an overall increase in admittance in the frequency range of 10 kHz $\leq f \leq$ 100 kHz.

* Based on an amplified, back-biased diode. This proved superior to some commercial white noise generators that were also tried.

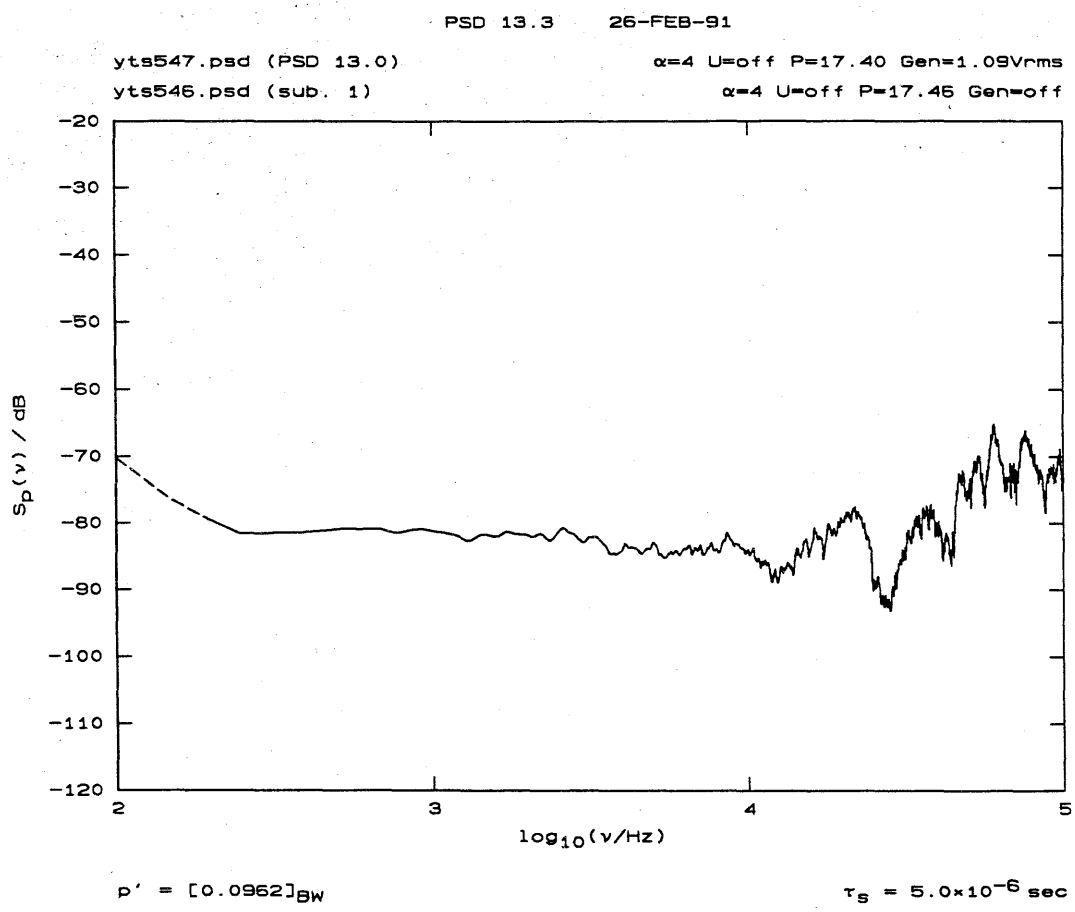

FIG. 10 Tunnel response to white noise excitation of lower guidewall acoustic transmitter (projector). Fluid at rest with hydrofoil at $\alpha = 4°$. Resulting admittance spectrum computed from that of Run 547, with the background noise spectrum of Run 546 subtracted.

It should be noted that the admittance spectrum plotted in Fig. 10 represents the admittance of the acoustical path from the transmitter to the receiver in the Tunnel. Being also dependent on the geometrical configuration in the Tunnel, it is also a function of the orientation (angle of attack) of the hydrofoil.

It is noted here that the acoustic admittance between acoustic sources located at the hydrofoil (test section mid-height) and the receiver would be different. No provision was made to measure *that* admittance in this test, as would be required for properly normalizing the acoustic spectrum data for a given Tunnel configuration. It should be noted that such a calibration measurement of the Tunnel admittance is certainly possible, but would have required a special side-wall window to be designed and fabricated for the purpose**.

** Such an undertaking was beyond what was realistically feasible for this test, given the bud-

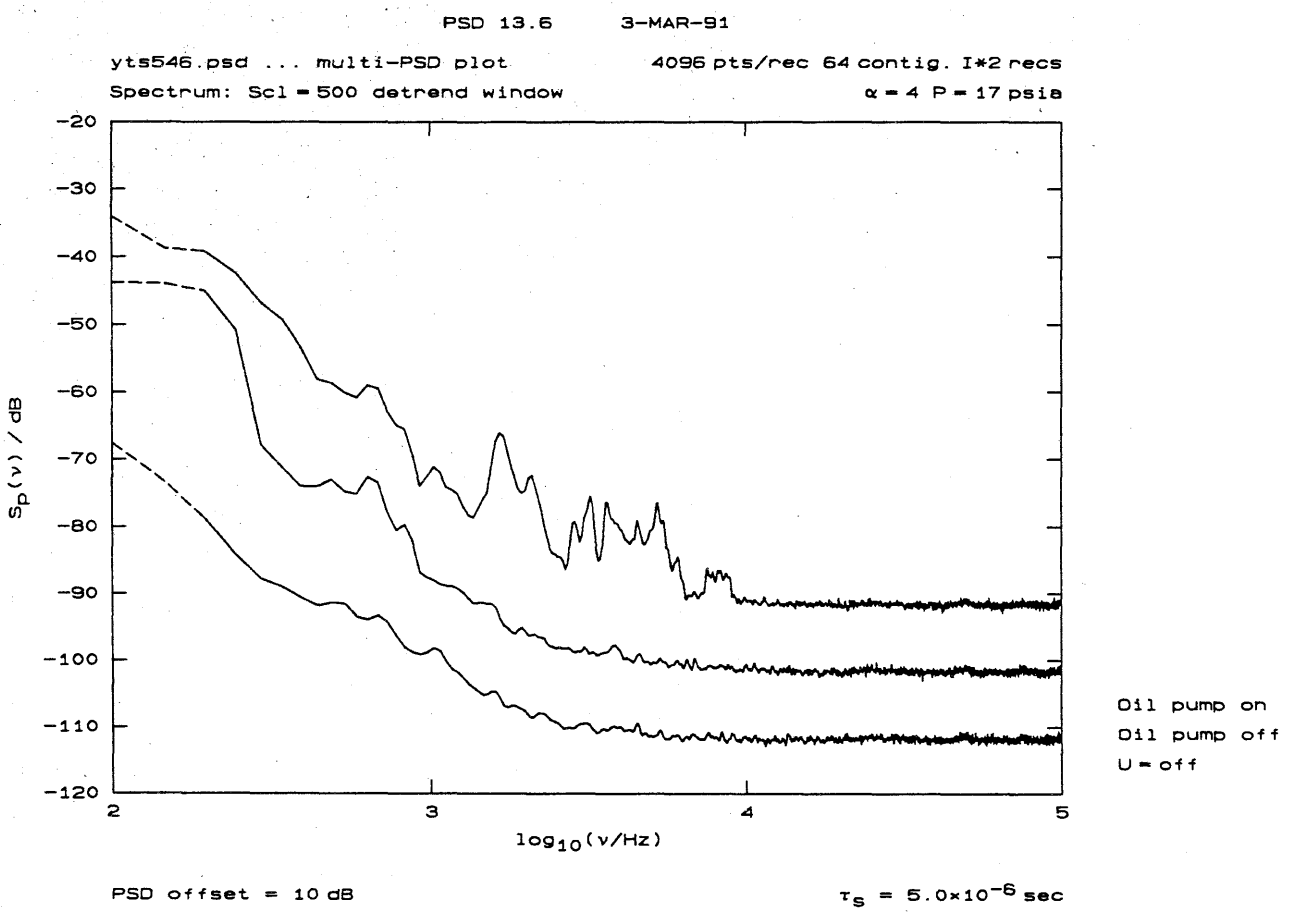

FIG. 11 Background noise spectrum data, recorded with Tunnel motor off and 7 rpm, the latter with the main bearing oil pump turned on (Run 548: top spectrum) and off (Run 550: middle spectrum). Bottom spectrum with Tunnel electrical machinery off (Run: 546). Spectra offset by 10 dB.

In the course of the 90–4 run sequence, we were also able to trace the Tunnel machinery acoustic noise contribution, apparent in Fig. 3, to the Tunnel motor main bearing oil pump. Similar features can be seen to persist in the top spectrum in Fig. 11, computed from the data in Run 548 (see sequence log listing on p. 16). It was decided, however, that the bearing oil pool was sufficiently large, that the oil pump could be turned off for the short time during which the hydroacoustic data were being recorded, thereby eliminating this extraneous noise source. Accordingly, a remote control system was installed, permitting this to take place relatively easily. The resulting hydroacoustic spectrum is the middle trace plotted in Fig. 11, recorded with the Tunnel motor running at 7 rpm, as before, with the main bearing oil pump turned off for the few seconds of hydroacoustic data recording (Run 550). As can be seen, the machinery noise is absent from the spectrum, with the background noise

getary constraints placed on the level of effort that could be expended.

ground noise now dominated by the electronic and other non-Tunnel noise that is recorded with the Tunnel machinery turned off†. The Tunnel bearing oil pump was turned off, as a matter of course, for all the subsequent hydroacoustic runs.

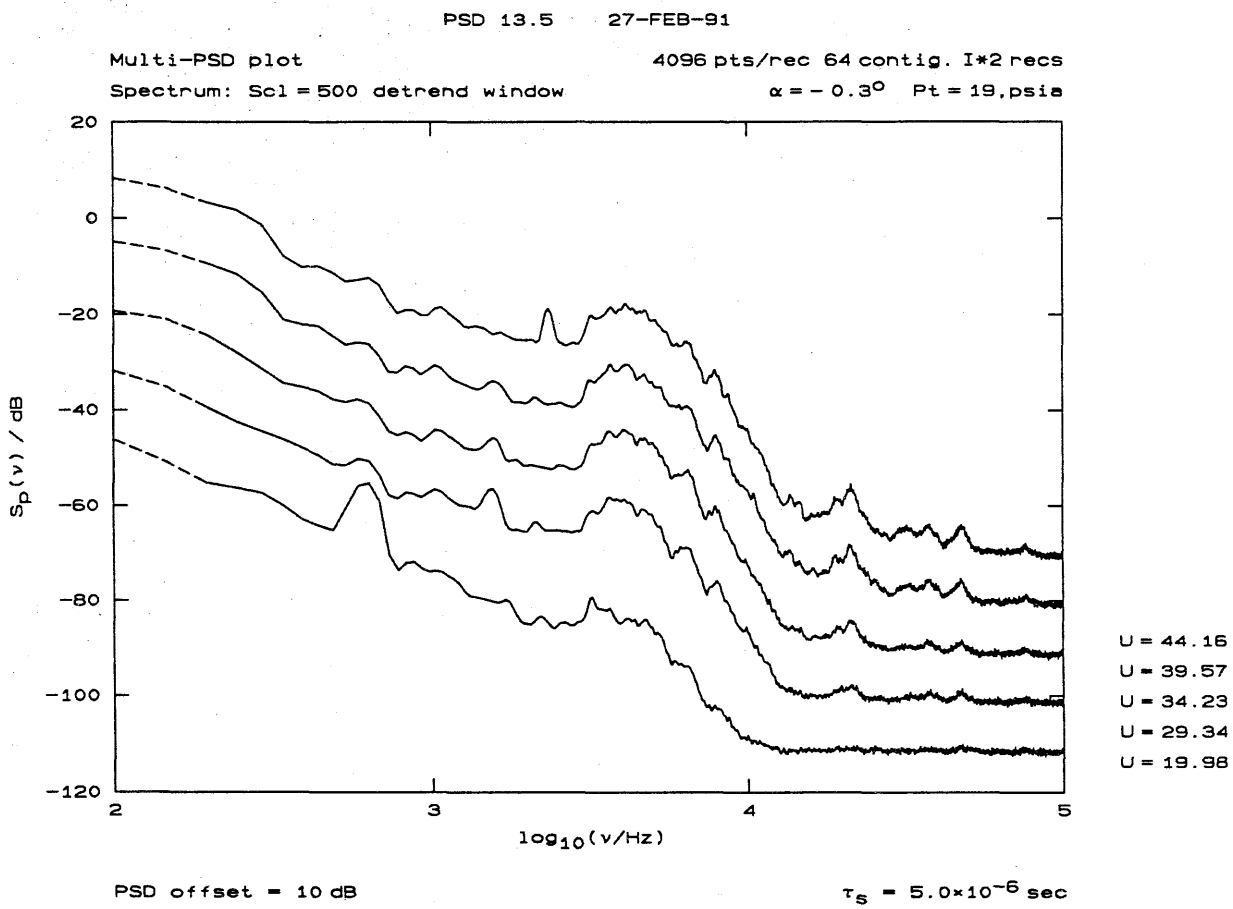

FIG. 12 Hydroacoustic spectra recorded with $\alpha = -0.3°$, with 16.5 psia $\leq p_{\text{test}} \leq$ 20.06 psia (Runs 551 through 555). Tunnel speed (ft/s) as indicated in plot legend, bottom right.

Finally, the hydrofoil was returned to an angle of attack of $\alpha = -0.3°$ and a Tunnel speed scan was made, with the Tunnel test section pressure held in the range 16.5 psia $\leq p_{\text{test}} \leq$ 20.06 psia. The resulting hydroacoustic spectra are plotted in Fig. 12. All data were recorded with the same amplifier gain setting (500). These represent the raw spectra computed for these runs, *i.e.* the small background noise was not subtracted and the admittance compensation was not applied. The increasing acoustic power content at high frequencies, as the speed

† Except for an intermittent contribution at low frequencies ($\sim$ 120 Hz) that was not always present, which we were not able to trace.

is increased, is evident. No cavitation is anticipated at these flow conditions and hydrofoil angle of attack.

3.5 20 July 1990: 90-5

In the next run sequence, the hydrofoil was set to $\alpha = 4°$. A run (556) was made at $U_{\text{test}} = 34\,\text{ft/s}$, followed by two test section pressure scans at $U_{\text{test}} \simeq 39\,\text{ft/s}$ and $U_{\text{test}} \simeq 20\,\text{ft/s}$. The log file is listed below.

YTSlog.0590 20-Jul-90 Filletted foil.
Air = 12.1, 12.3 ml/l.

run	alpha	P/psia	U/(ft/s)	Gain	Comments
556	4.0	19.82	34.00	500	212 rpm
%					
557	4.0	27.68	39.10	500	243 rpm
558	4.0	24.71	39.04	500	
559	4.0	17.85	39.02	200	
560	4.0	14.19	38.99	200	
561	4.0	12.36	38.95	200	
562	4.0	10.46	39.05	200	
563	4.0	9.82	38.99	200	
564	4.0	9.12	38.94	200	
565	4.0	18.74	39.25	500	A few points below min A/D count
%					
566	4.0	24.84	19.87	500	124 rpm
567	4.0	9.95	19.78	500	
568	4.0	6.97	19.71	500	
569	4.0	5.95	19.56	500	
570	4.0	5.07	19.77	500	
571	4.0	4.97	19.68	500	
572	4.0	3.99	19.77	500	
573	4.0	3.06	19.59	500	
574	4.0	2.84	19.59	500	
575	4.0	2.67	19.72	500	
576	4.0	2.00	19.48	500	Supercavitation

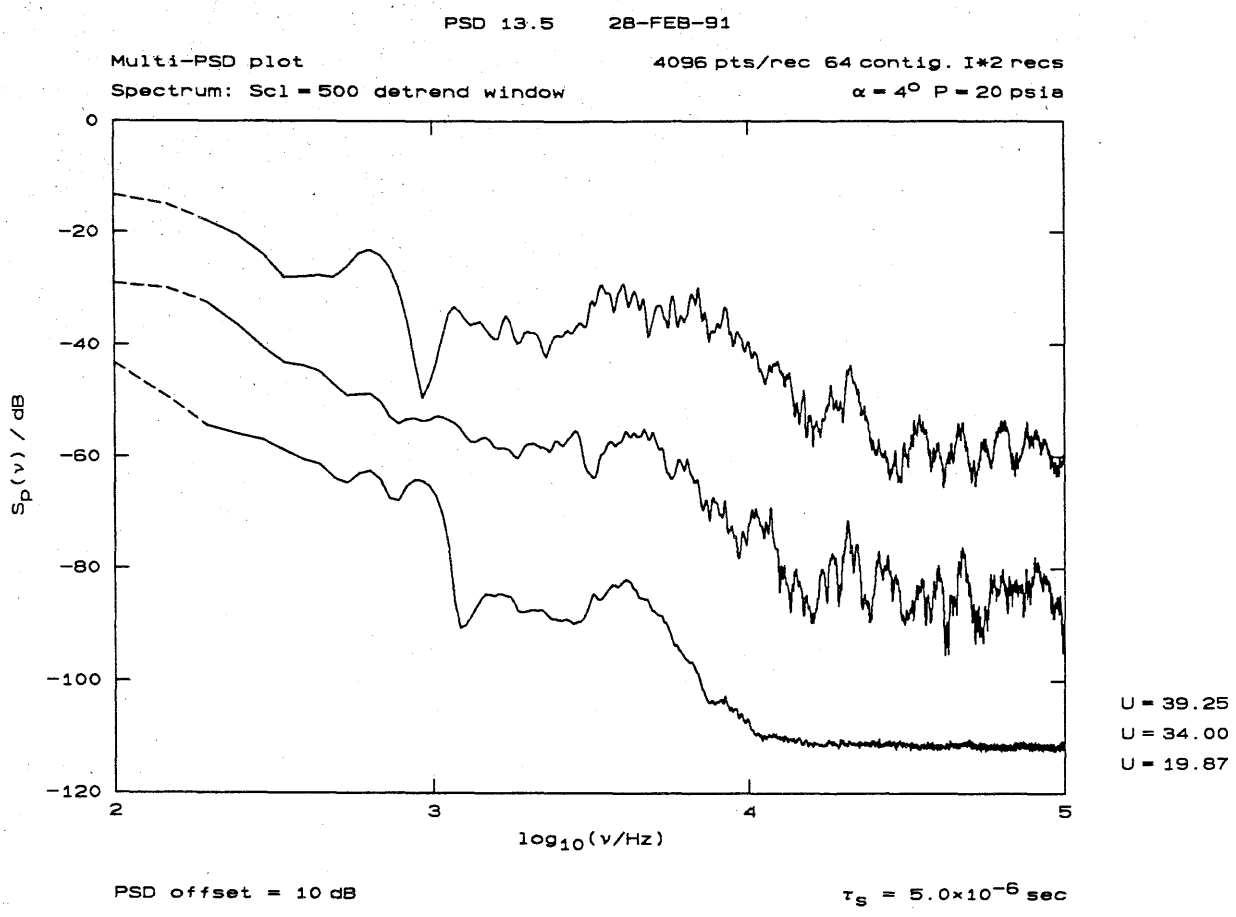

FIG. 13 Hydroacoustic spectra at $\alpha = 4°$ and $p_{\text{test}} \simeq 20\,\text{psia}$. Tunnel speed as indicated in plot legend, bottom right. Note that successive spectra are offset by 10 dB.

Figure 13 plots the hydroacoustic spectra at $U_{\text{test}} = 19.87$, 34.00, and 39.25 ft/s; from Runs 566, 556 and 565; respectively. The Tunnel test section pressure was $p_{\text{test}} \simeq 20\,\text{psia}$. The rise in the high frequency, *i.e.*

$$10\,\text{kHz} \leq f \leq 100\,\text{kHz} ,$$

spectral content, as Tunnel speed is increased, is the conspicuous signature of cavitation. It should be compared to the corresponding behavior in the Tunnel speed scan in Fig. 12, for $\alpha = -0.3°$ and comparable test section pressure.

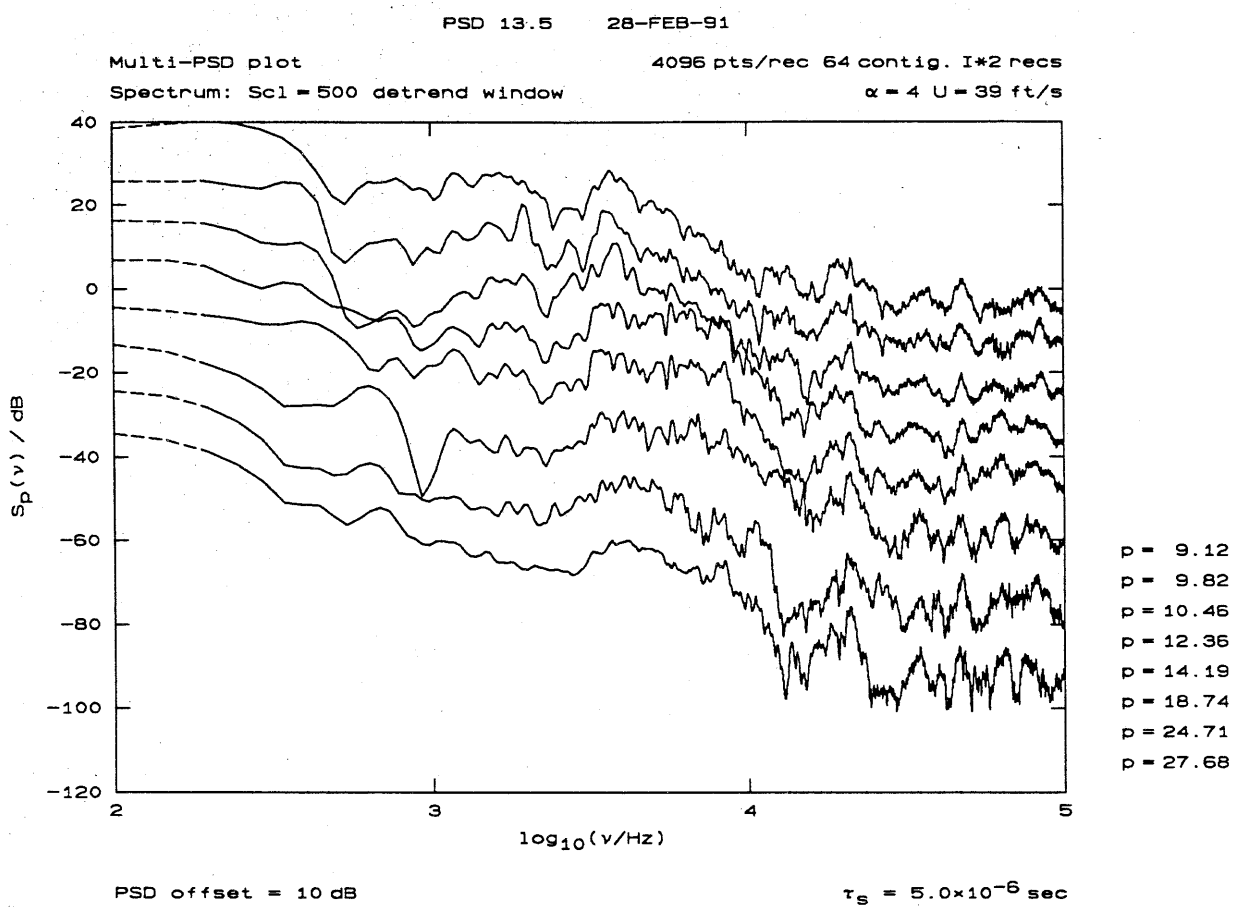

FIG. 14 Hydroacoustic spectra at $\alpha = 4°$ and $U_{\text{test}} = 39\,\text{ft/s}$ as a function of test section pressure. Tunnel pressure (psia) as indicated in plot legend, bottom right. Successive spectra are offset by 10 dB.

The hydroacoustic spectra for the pressure scan at $U_{\text{test}} \simeq 39\,\text{ft/s}$ (Runs 557–565) are plotted in Fig. 14. At this Tunnel speed and angle of attack, the high frequency cavitation signature can be found at the highest pressure that was included in these data and increases as the pressure (cavitation number) decreases.

The hydroacoustic spectra for the pressure scan at $U_{\text{test}} \simeq 20\,\text{ft/s}$ (Runs 566–576) are plotted in Fig. 15. This is an interesting sequence. At this low speed, the flow noise is much reduced and the onset of cavitation ($5.95\,\text{psia} < p_{\text{test}} < 5.07\,\text{psia}$) results in a dramatic increase in the hydroacoustic spectral content in the frequency range of $10\,\text{kHz} \leq f \leq 100\,\text{kHz}$. There is a second dramatic increase that occurs at the lowest pressure ($p_{\text{test}} = 2.00\,\text{psia}$) that is the result of hydrofoil supercavitation, as noted in the run sequence log (p. 20).

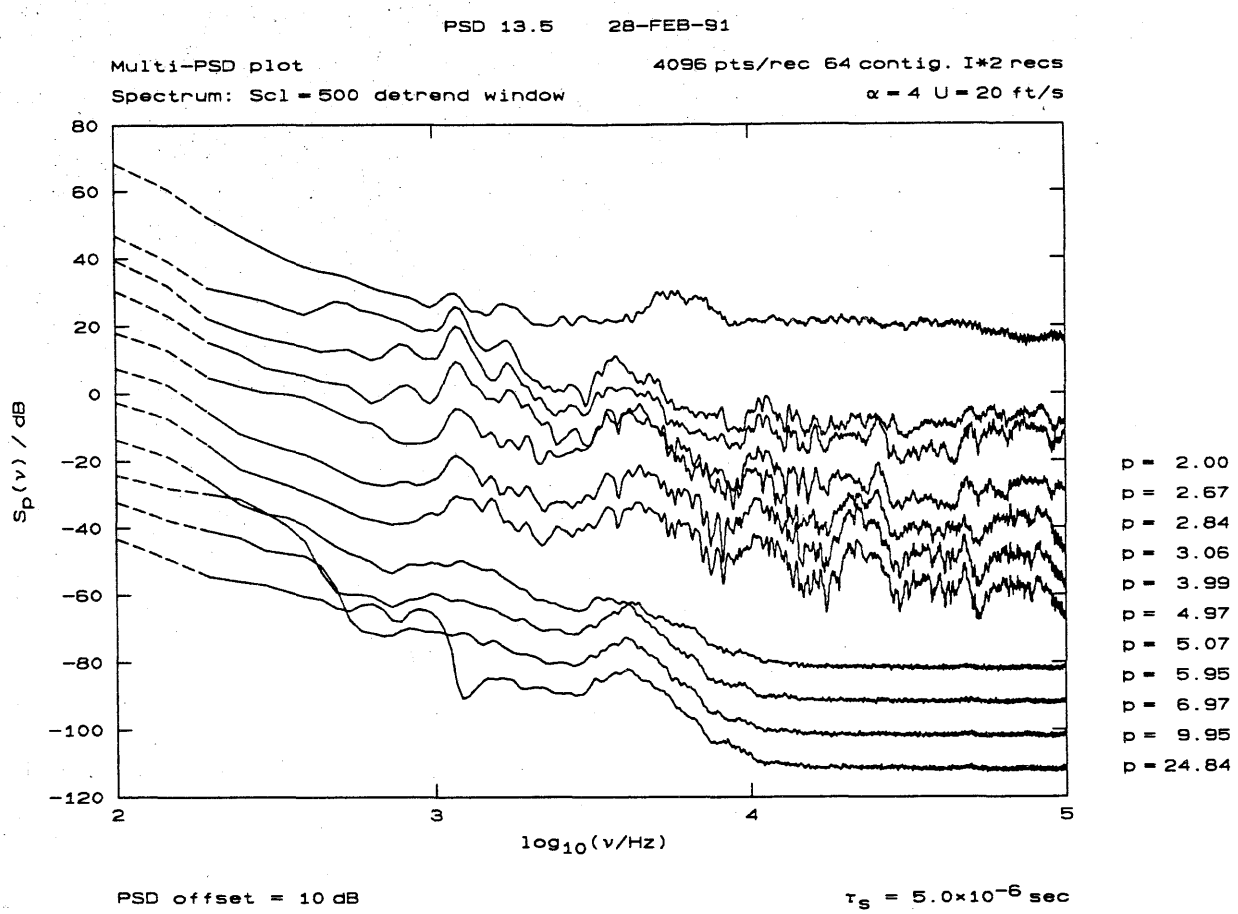

FIG. 15 Hydroacoustic spectra at $\alpha = 4°$ and $U_{\text{test}} = 20\,\text{ft/s}$ as a function of test section pressure. Tunnel pressure (psia) as indicated in plot legend, bottom right. Successive spectra are offset by 10 dB.

The spectra in this sequence are also interesting on another count. For all but the lowest pressure, this flow configuration appears to have excited the fundamental standing wave resonance, corresponding to a half acoustic wavelength across the test section height ($f \approx 1\,\text{kHz}$)‡. Its amplitude, however, is substantially weakened at the lowest pressure, where supercavitation was observed. This can be understood by appreciating that, under supercavitating flow conditions, which will want to force a node at mid-height, this mode can be expected to be very highly damped in the test section.

‡ Recall that the test section height is $h = 32'' = 0.762\,\text{m}$.

3.6 23 July 1990: 90-6

The hydrofoil was set to $\alpha = 6°$ angle of attack for the next run sequence. New background reference noise data were recorded with the Tunnel motor both on and off (Runs 577 and 578, respectively). A test section pressure scan was then made holding the Tunnel speed constant to $U_{\text{test}} \simeq 20\,\text{ft/s}$ and a smaller scan at $U_{\text{test}} \simeq 39\,\text{ft/s}$. The log file `YTSlog.0690` is listed below.

```
YTSlog.0690     23-Jul-90                Filletted foil
                                         Air = 12.8 ml/l.
-------------------------------------------------------------------------------
run    alpha   P/psia  U/(ft/s) Gain    Comments
-------------------------------------------------------------------------------
577     6.0     21.92     off    500
578     6.0     21.84    7rpm    500
579     6.0     14.96    19.97   500    111 rms (A/D counts)            %s=5.53
580     6.0     11.90    19.97   500    115 rms                         %s=4.39
581     6.0      8.95    19.82   500    120 rms                         %s=3.26
582     6.0      7.95    19.71   500    109 rms                         %s=2.88
583     6.0      6.91    19.80   500    151 rms                         %s=2.50
584     6.0      6.03    19.89   500    145 rms                         %s=2.12
585     6.0      5.02    19.95   500    171 rms                         %s=1.74
586     6.0      4.02    19.71   500    274 rms  1.35" < Lc < 1.5"      %s=1.36
587     6.0      2.94    19.69    50    181 rms  Unstable cavity.       %s=1.74
%
588     6.0      2.94    20.02    50    185 rms  BW=.3Hz-1kHz,  Clock=2kHz.
589     6.0     15.69    7rpm    500    115 rms  BW=.3Hz-1kHz,  Clock=2kHz.
%
590     6.0     34.35    39.51   500    A few points below min A/D count
591     6.0     31.23    39.28   100    Cav. on thin lines behind LE
592     6.0     28.93    38.93   100    Lines ~ 1/8" behind LE
593     6.0     27.03    39.24   100    Lc > 1/4"
594     6.0     19.01    39.05    20    Lc > 3/4"
-------------------------------------------------------------------------------
```

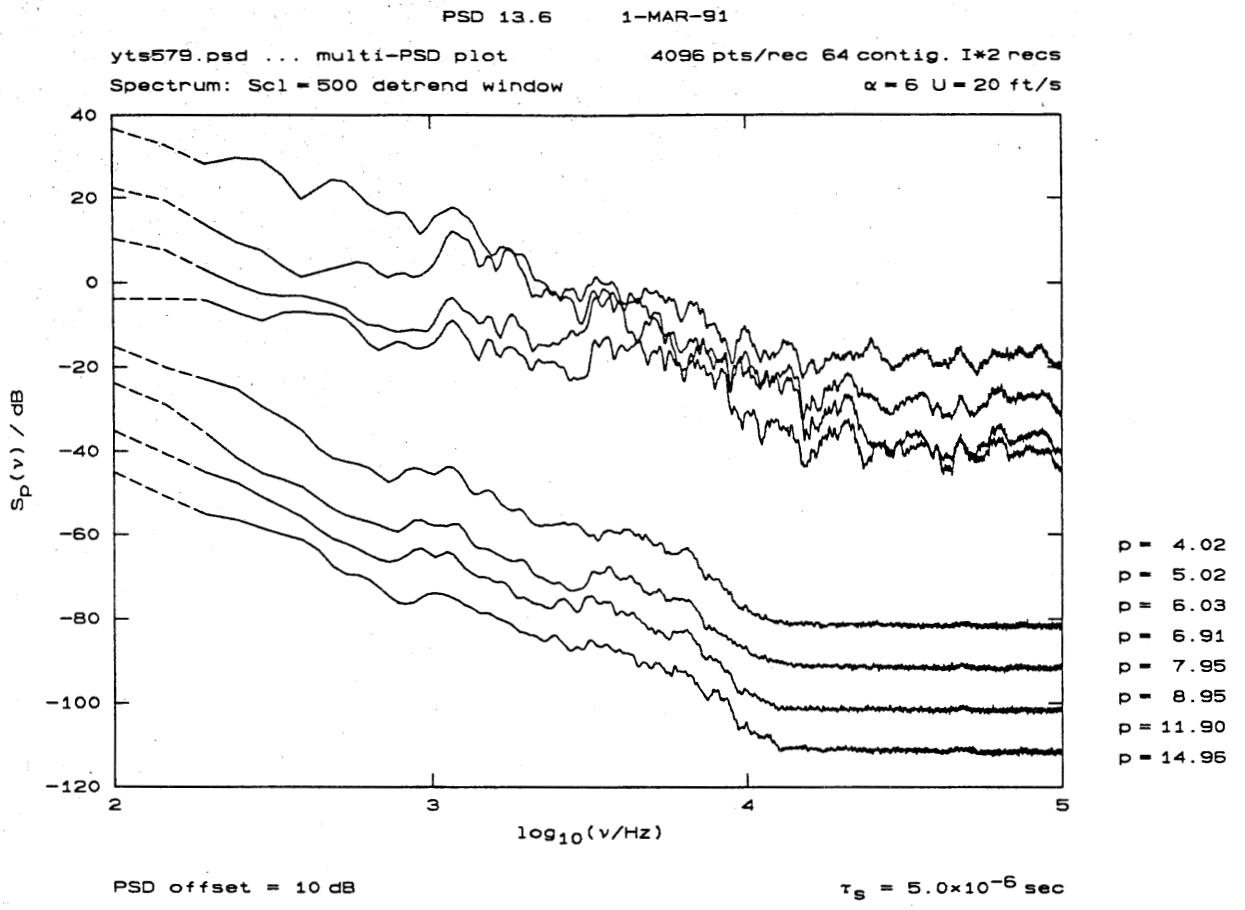

FIG. 16 Hydroacoustic spectra at $\alpha = 6°$ and $U_{\text{test}} \simeq 20\,\text{ft/s}$. Tunnel pressure as indicated in plot legend, bottom right. Successive spectra are offset by 10 dB.

Figure 16 plots the hydroacoustic spectra at $U_{\text{test}} \simeq 20\,\text{ft/s}$ in the pressure range $4.02\,\text{psia} \leq p_{\text{test}} \leq 14.96\,\text{psia}$ (Runs 579–586)*. As with the similar scan at $\alpha = 4°$ (Fig. 15), the onset of cavitation is unmistakable.

* Run 587 was recorded at a much lower amplifier gain and, as a consequence, was characterized by a much lower (electronic) signal to noise ratio at high frequencies. It was not included in this plot. See `YTlog.0690` log listing on p. 24.

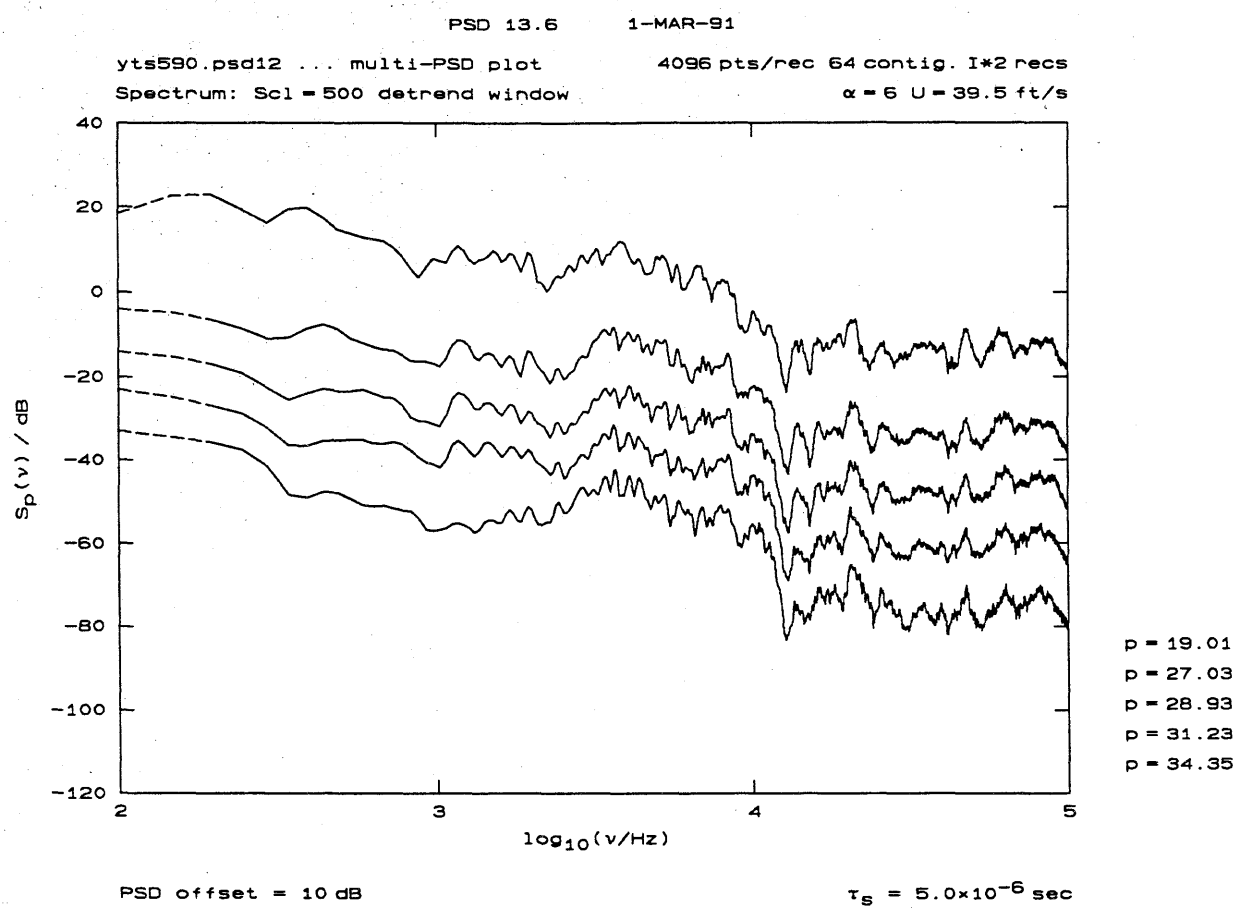

FIG. 17 Hydroacoustic spectra at $\alpha = 6°$ and $U_{\text{test}} \simeq 40\,\text{ft/s}$. Tunnel pressure as indicated in plot legend, bottom right. Successive spectra are offset by 10 dB.

Figure 17 plots the hydroacoustic spectra at $U_{\text{test}} \simeq 40\,\text{ft/s}$ in the pressure range $19.01\,\text{psia} \leq p_{\text{test}} \leq 34.35\,\text{psia}$ (Runs 590–594). At this Tunnel speed, the hydroacoustic evidence is that there was some cavitation even at the highest pressure (cavitation number). In this case, this was also corroborated by visual (stroboscopic) evidence**.

** Spotty (very small regions), leading edge cavitation.

3.7 24 July 1990: 90-7

The hydrofoil was set to $\alpha = 2°$ angle of attack for the next run sequence. New background reference noise data were recorded with the Tunnel motor both on and off (Runs 595–598). A test section pressure scan was then made holding the Tunnel speed constant to $U_{test} \simeq 20\,\mathrm{ft/s}$ and a smaller scan at $U_{test} \simeq 30\,\mathrm{ft/s}$. The log file `YTSlog.0790` for these runs is listed below.

```
YTSLOG.0790     24-Jul-90       A/C fans also off.
                                Air = 11.8, 12.1 ml/l
-------------------------------------------------------------------------------
run    alpha   P/psia  U/(ft/s) Gain    Comments
-------------------------------------------------------------------------------
595     2.0     14.09     off   1000    P = 2.409'Hg
596     2.0     13.96    7rpm   1000
597     2.0     13.93    7rpm    500
598     2.0     13.96    7rpm    200
%
599     2.0     14.87   20.14   1000
600     2.0      9.93   20.06   1000
601     2.0      7.51   20.22   1000
602     2.0      4.98   20.19   1000
603     2.0      3.93   20.25   1000
604     2.0      2.94   20.07   1000
605     2.0      2.02   19.94   1000    Tip-gap cavitation
606     2.0      1.83   19.69    500
%
607     2.0     14.83   29.99    500
608     2.0      9.93   29.92    500
609     2.0      7.53   29.80    500
610     2.0      5.04   29.83    500
611     2.0      4.06   29.99    500    Root cavitation
612     2.0      3.07   29.91     50    Strong root cavitation
613     2.0     14.90    7rpm     50    rms = 14 A/D cts
-------------------------------------------------------------------------------
```

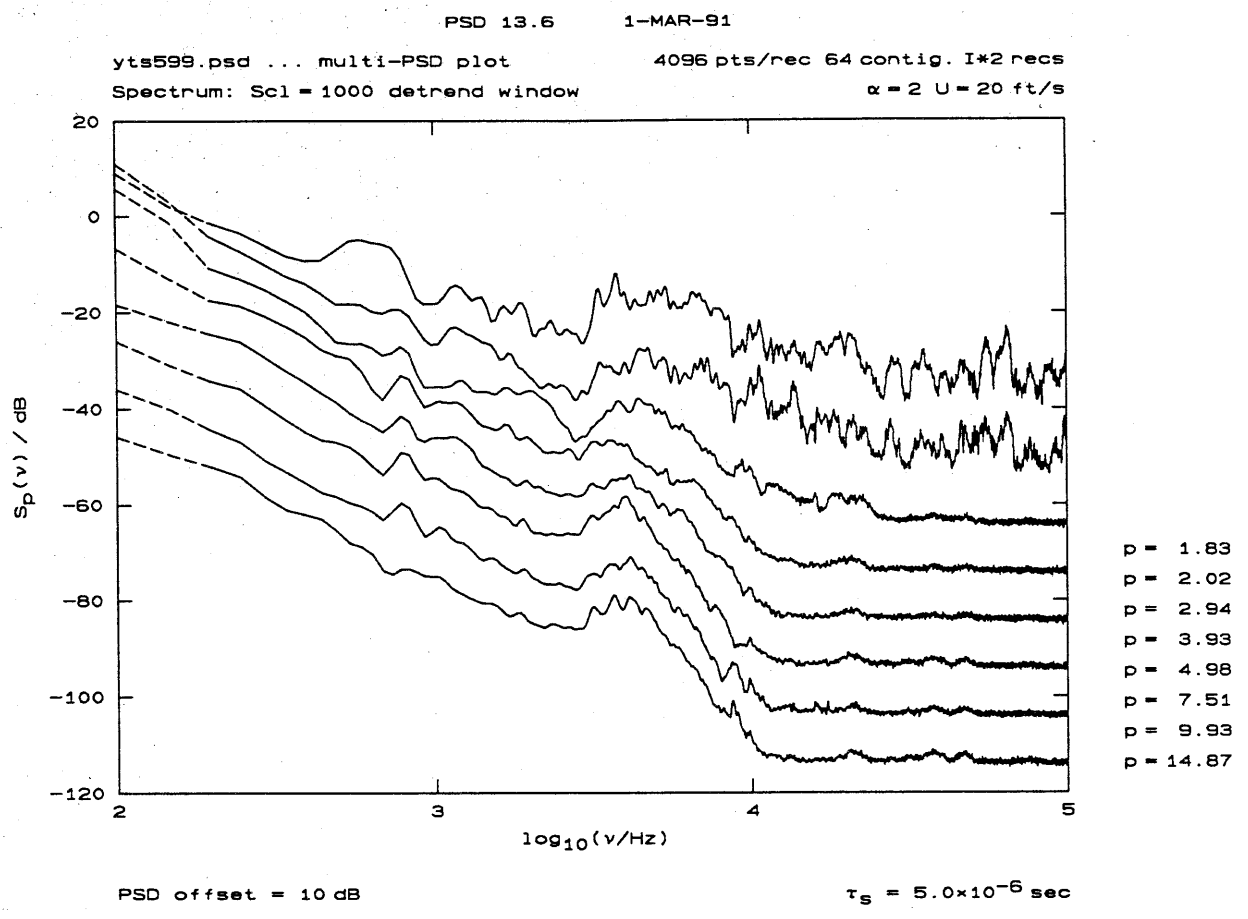

FIG. 18 Hydroacoustic spectra at $\alpha = 2°$ and $U_{\text{test}} \simeq 20\,\text{ft/s}$. Tunnel pressure as indicated in plot legend, bottom right. Successive spectra offset by 10 dB.

Figure 18 plots the hydroacoustic spectra at $U_{\text{test}} \simeq 20\,\text{ft/s}$ in the pressure range $1.83\,\text{psia} \leq p_{\text{test}} \leq 14.87\,\text{psia}$ (Runs 599–606).

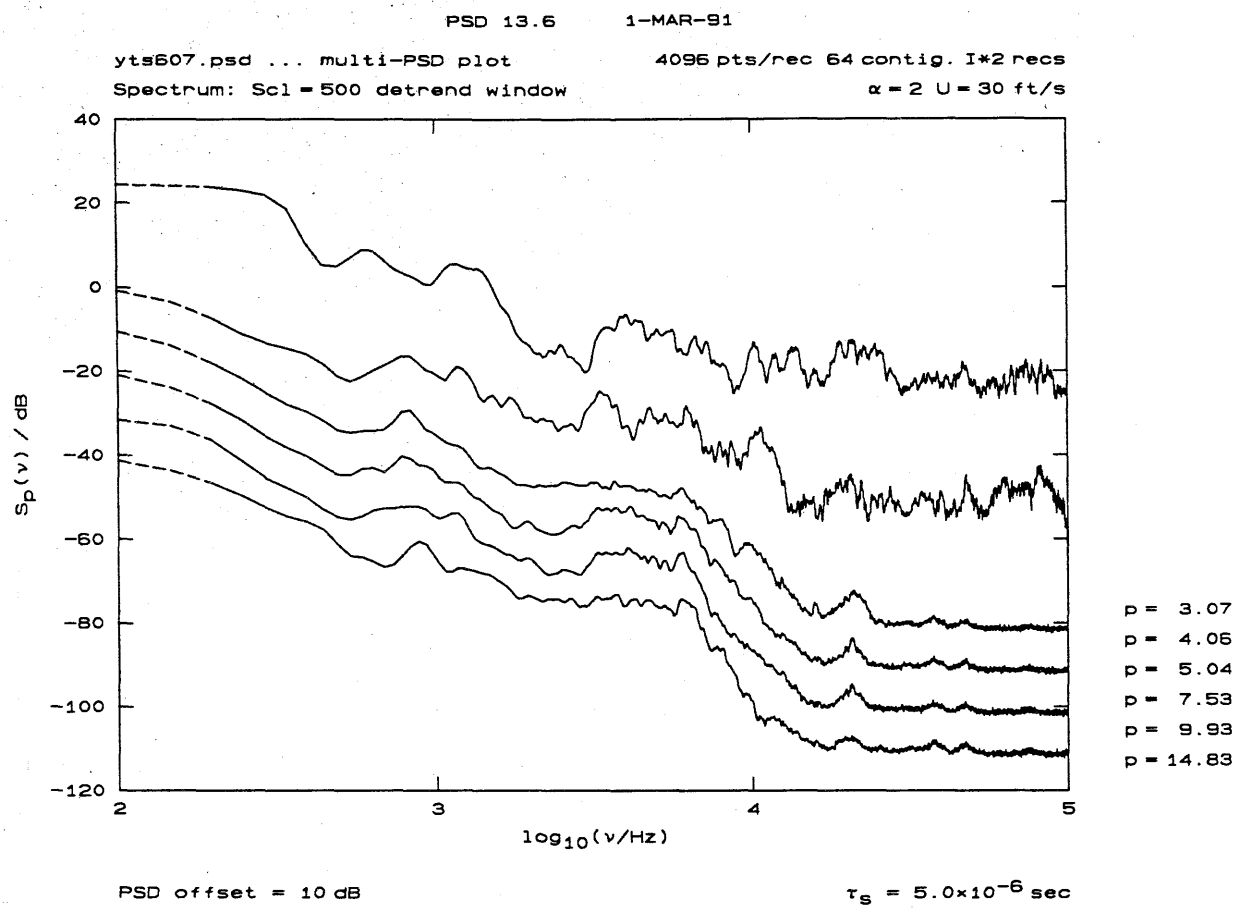

FIG. 19 Hydroacoustic spectra at $\alpha = 2°$ and $U_{\text{test}} \simeq 30\,\text{ft/s}$. Tunnel pressure as indicated in plot legend, bottom right. Successive spectra offset by 10 dB.

Figure 19 plots the hydroacoustic spectra at $U_{\text{test}} \simeq 30\,\text{ft/s}$ in the pressure range $3.07\,\text{psia} \leq p_{\text{test}} \leq 14.83\,\text{psia}$ (Runs 607–613). Please note that the spectrum at the lowest pressure (top trace) was recorded with an amplifier gain one tenth that of the other runs (*cf.* `ytslog.0790` log listing on p. 27). As a consequence, a (small) part of the difference in the spectrum level is attributable to the corresponding relative increase in electronic noise.

3.8 24 July 1990: 90-8

The hydrofoil was returned to $\alpha = 6°$ angle of attack, for the next test sequence, to record a pressure scan run sequence, at an intermediate Tunnel speed of $U_{\text{test}} \simeq 30\,\text{ft/s}$ (*cf.* `ytslog.0690` run sequence listing, p. 24).

YTSLOG.0890 24-Jul-90 %a=6, U=30 ft/s
Air = 11.8, 12.1 ml/l

run	alpha	P/psia	U/(ft/s)	Gain	Comments
614	6.0	40.27	29.67	500	
615	6.0	34.55	29.22	500	
616	6.0	31.77	29.39	500	Occasional hissing
617	6.0	29.68	29.18	500	
618	6.0	24.87	29.32	500	
619	6.0	19.71	29.29	500	Hissing/crackling traced to root (vis.)
620	6.0	17.75	29.36	500	Gap cavitation + LE spot.
621	6.0	15.89	29.16	200	Gap + LE cavitation
622	6.0	13.95	29.33	200	Lc=0.4"
623	6.0	11.89	29.15	200	Lc=0.65"
624	6.0	9.99	29.10	100	Lc=1.25"
625	6.0	7.93	29.17	50	Lc=2.4"
626	6.0	7.49	29.05	50	Lc=0.6c
627	6.0	19.47	7rpm	100	

Additional care was expended to allow the test section pressure to start at a high value of $p_{\text{test}} \approx 40\,\text{psia}$ (*cf.* Run 614).

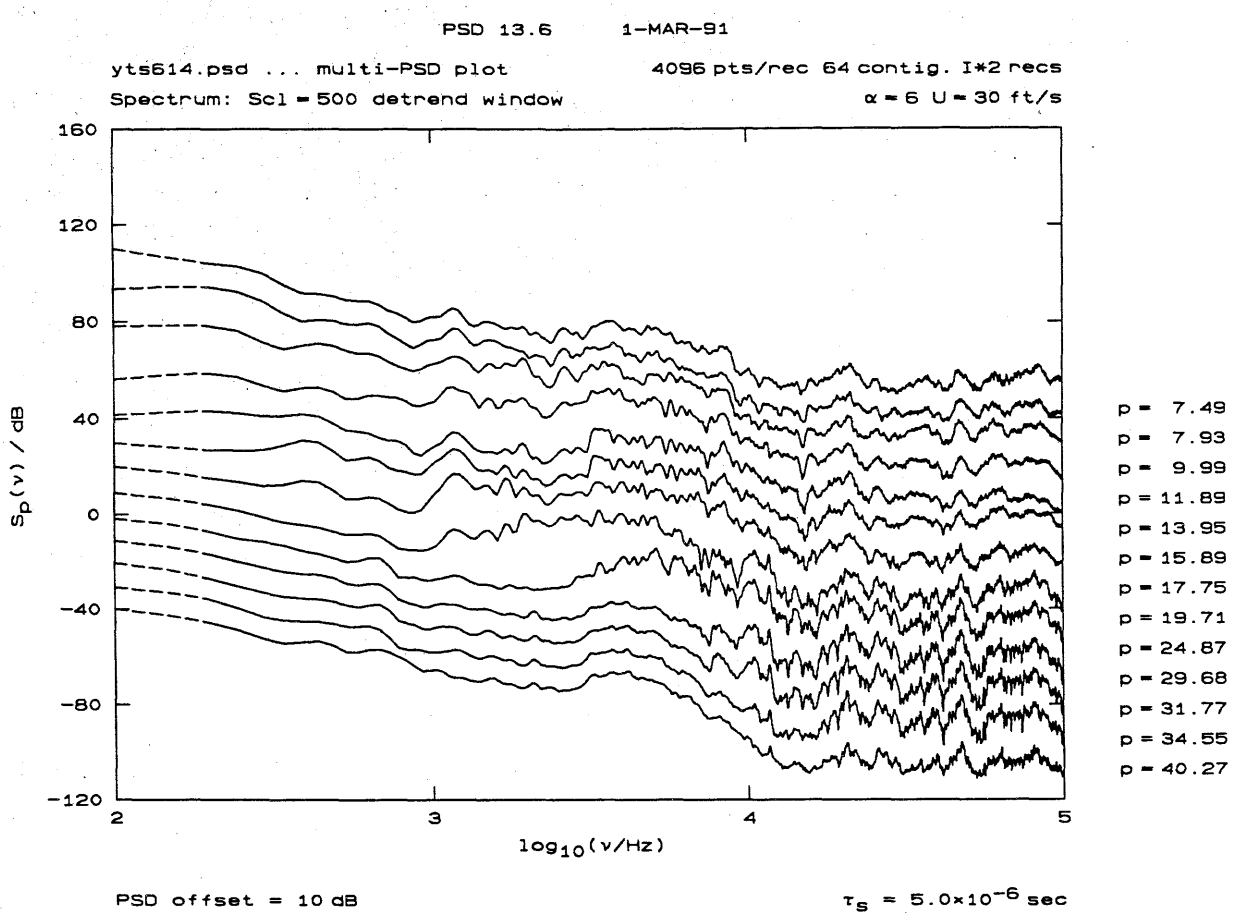

FIG. 20 Hydroacoustic spectra at $\alpha = 6°$ and $U_{\text{test}} \simeq 30\,\text{ft/s}$. Tunnel pressure as indicated in plot legend, bottom right. Successive spectra offset by 10 dB.

Figure 20 plots the resulting hydroacoustic spectra at $U_{\text{test}} \simeq 30\,\text{ft/s}$, in the pressure range $7.49\,\text{psia} \leq p_{\text{test}} \leq 40.27\,\text{psia}$ (Runs 614–626). As can be seen, the hydroacoustic evidence suggests that some cavitation was present at the highest pressure ($p_{\text{test}} = 40.27\,\text{psia}$). No visible indications of this were available. A faint, intermittent, high frequency hissing could be heard at $p_{\text{test}} \simeq 32\,\text{psia}$. This became more pronounced by $p_{\text{test}} \simeq 20\,\text{psia}$, where, on the basis of the first (stroboscopic) visual evidence, the cavitation was identified as occurring at the hydrofoil root.

3.9 25 July 1990: 90-9

To investigate the effects of air content, the hydrofoil was left at an $\alpha = 6°$ angle of attack and the Tunnel was run at high speed for some time, under low pressure, admitting substantial air into the test section through a pair of static pressure taps. Additionally, the hydrofoil gap gasket was recemented and trimmed to be more closely edged to the hydrofoil thickness contour. The pressure scan at $U_{\text{test}} \simeq 30\,\text{ft/s}$ was then repeated, starting at an even higher pressure $p_{\text{test}} \simeq 44.5\,\text{psia}$. The test sequence log file is listed below.

```
YTSLOG.0990     25-Jul-90       %a=6,  U=30 ft/s
                                High air content = 16.2, 16.7 ml/l
                                Recement gap gasket
-------------------------------------------------------------------------------
run    alpha   P/psia  U/(ft/s) Gain    Comments
-------------------------------------------------------------------------------
628     6.0    15.44     off    500
629     6.0    15.39    7rpm    500
%
630     6.0    44.64   29.40    500    No visible cavitation
631     6.0    39.57   29.23    500    No visible cavitation
632     6.0    34.86   29.19    500    No visible cavitation
633     6.0    29.75   29.42    500    No visible cavitation. Hissing.
634     6.0    32.20   29.34    500    No visible cavitation. Hissing.
635     6.0    24.85   29.32    500    Root cavitation.
636     6.0    19.82   29.35    500    Root cavitation.
                                       Intermittent cav. sheet at 18 psi
637     6.0    15.79   29.39    200    1/8" < Lc < 0.2"
638     6.0    12.05   29.17    200    Lc=0.1c
639     6.0     7.85   29.36    100    Lc=0.4c.  Fillet lost around mid-chord.
%
640     6.0    14.70    7rpm    200
-------------------------------------------------------------------------------
```

Figure 21 plots the resulting hydroacoustic spectra at $U_{\text{test}} \simeq 30\,\text{ft/s}$, in the pressure range $7.85\,\text{psia} \leq p_{\text{test}} \leq 44.64\,\text{psia}$ with the resulting elevated air content (Runs 630–639). As noted in the log, the hydroacoustic and other evidence indicated no cavitation at the highest and next two lower pressures ($p_{\text{test}} = 44.64$, 39.57, and 34.86 psia).

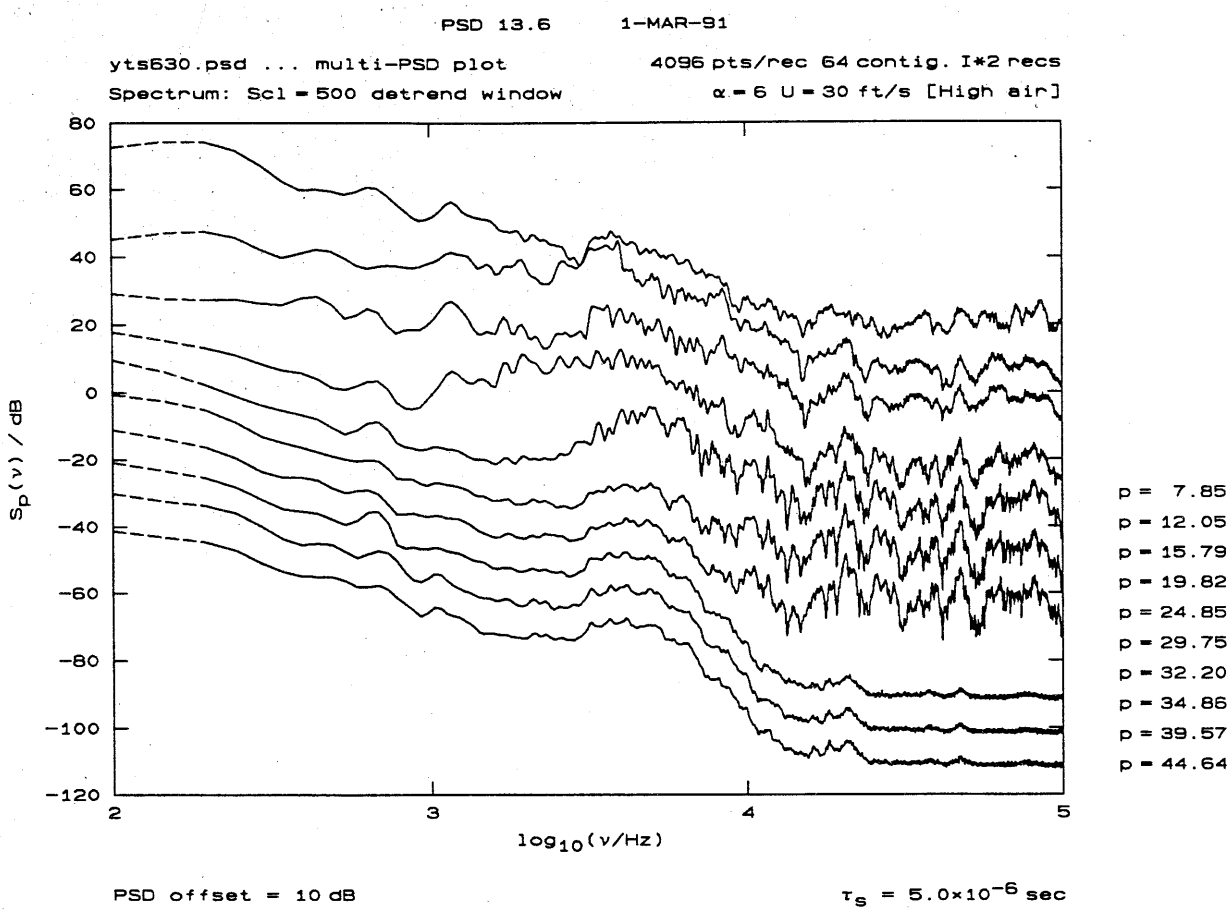

FIG. 21 Hydroacoustic spectra at $\alpha = 6°$ and $U_{\text{test}} \simeq 30\,\text{ft/s}$ at high air content. Tunnel pressure as indicated in plot legend, bottom right. Successive spectra offset by 10 dB.

As the air content was now *higher*, this was opposite to the expected behavior. While it is possible that the delay in cavitation inception, relative to that observed with a lower air content, could be attributed to the rather more careful trim and cementing of the tip gap gasket, a *decrease* in the length of the cavitation bubbles was also observed, as the Tunnel test section pressure was lowered.

3.10 26 July 1990: 90-10

The next set or runs represented further exploratory investigations of the acoustic admittance behavior with the hydrofoil mounted at different angles, as well as of the electronic and signal acquisition noise, using different amplifier gains and various signal grounding schemes.

The test sequence log for Runs 641 through 651 is listed below.

YTSLOG.1090 26-Jul-90 %a=6, U=30 ft/s
Air = 16.2 ml/l

run	alpha	P/psia	U/(ft/s)	Gain	Comments	
641	6.0	15.75	off	2000	Gen off. Hi lo-f noise	[1024 blocks]
642	6.0	15.60	off	2000	Gen at 1.06Vrms	[1024 blocks]
%						
643	6.0	39.44	29.21	2000		
644	6.0	34.76	29.28	2000		
645	6.0	34.70	29.25	1000		
646	6.0	32.24	29.35	1000		
647	6.0	29.97	29.20	1000		
648	6.0	16.11	off	1000	Background noise.	
649	6.0	16.09	off	2000	Background noise.	
%						
650	6.0	15.24	off	2000	Gen off. Background noise	[4096 blocks]
651	6.0	15.00	off	2000	Gen at 1.06Vrms	[4096 blocks]

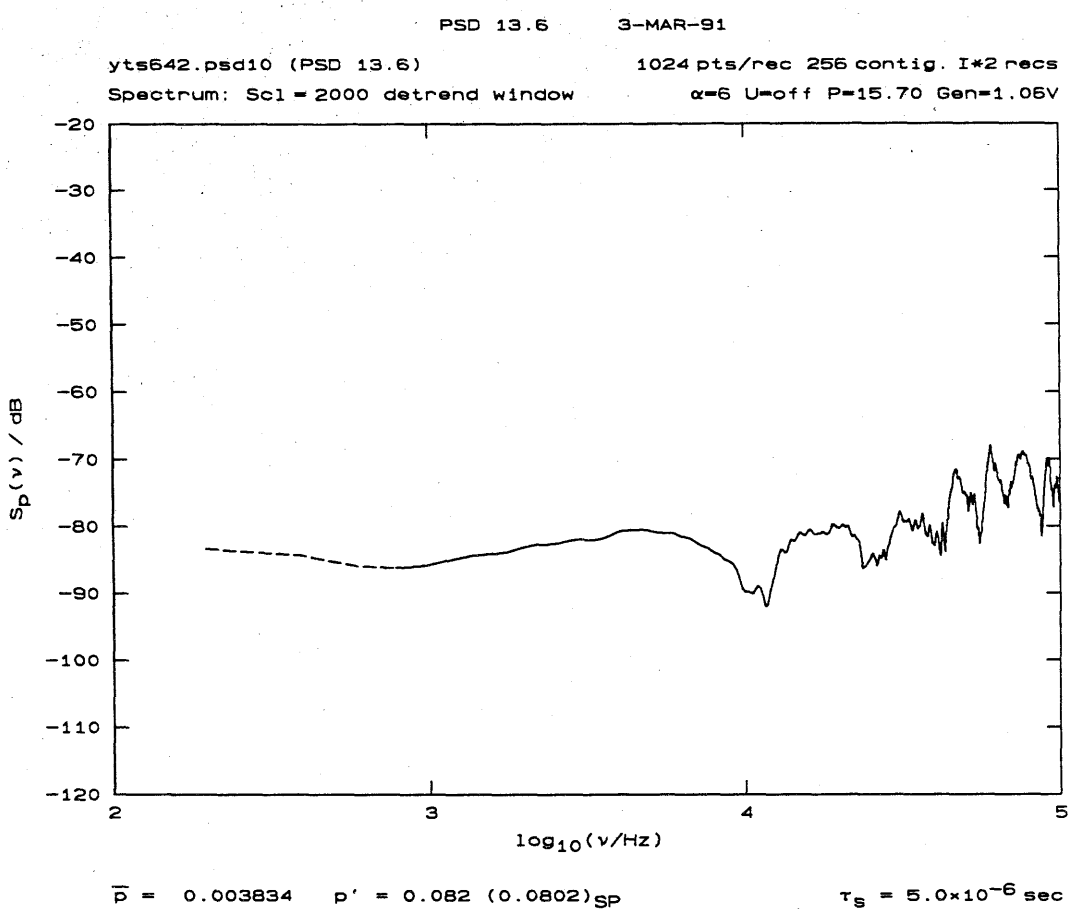

FIG. 22 Tunnel response to white noise excitation of lower guidewall acoustic transmitter (Run 642). Hydrofoil at $\alpha = 6°$. Spectrum is computed from contiguous $2^{10} = 1,024$ point records.

The acoustic admittance spectrum with the hydrofoil mounted at $\alpha = 6°$ is plotted in Fig. 22. This spectrum was computed by processing the data as comprised of (four times as many) contiguous records of $2^{10} = 1,024$ points each*. Comparing the high frequency end with that in Fig. 10, we can see that this admittance is (slightly) different from the one measured with the airfoil mounted at $\alpha = 4°$.

* The trade-off here is between statistical significance in the spectral estimate and frequency resolution.

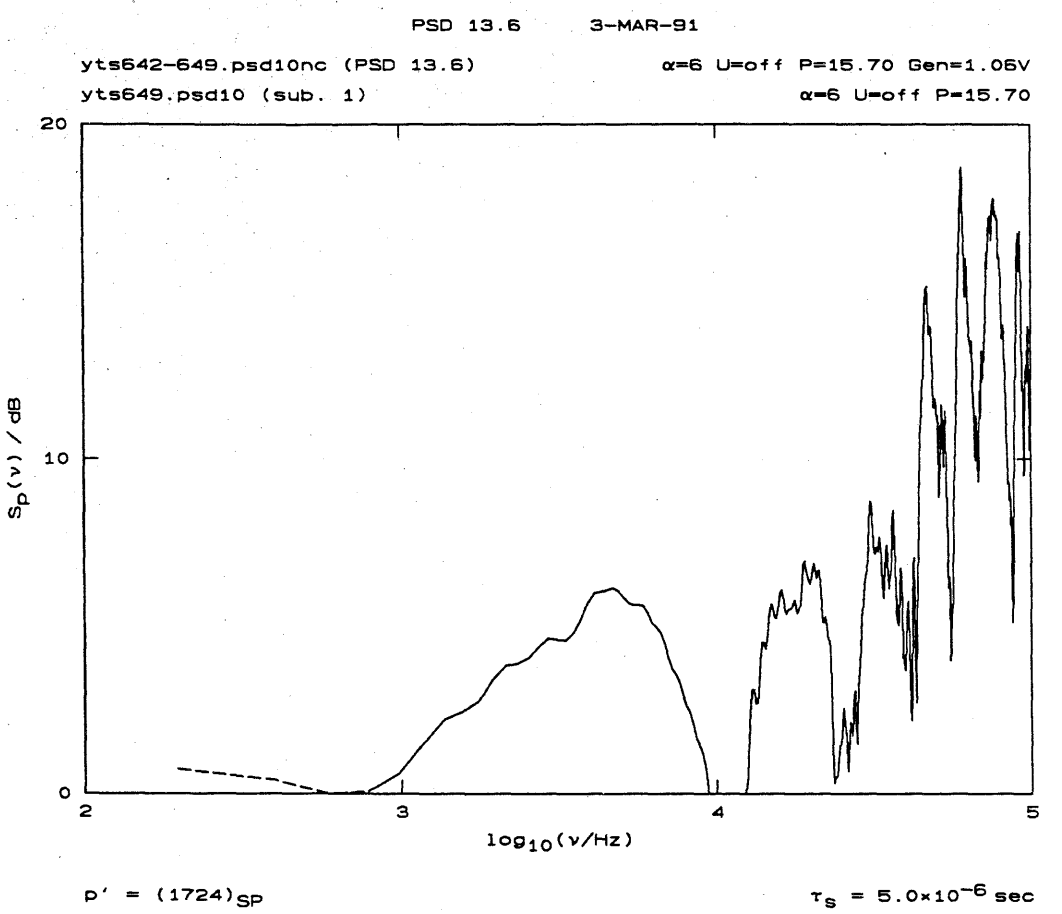

FIG. 23 Tunnel response to white noise excitation of lower guidewall acoustic transmitter (Run 642). Hydrofoil at $\alpha = 6°$. Spectrum is computed from contiguous, $2^{10} = 1,024$ point, records. Background noise (Run 649) subtracted. Spectrum normalized to 0 dB at its minimum for $f < 1$ kHz.

The background noise was subtracted from this spectrum (Run 649) and the difference was normalized to 0 dB at its minimum below $f = 1$ kHz**. The result is plotted in Fig. 23. The large variations in admittance with frequency are noteworthy.

** It was also truncated to 0 dB, as indicated in the plot. It was felt that resonances at high frequencies would be much more damped under actual flow/cavitation conditions.

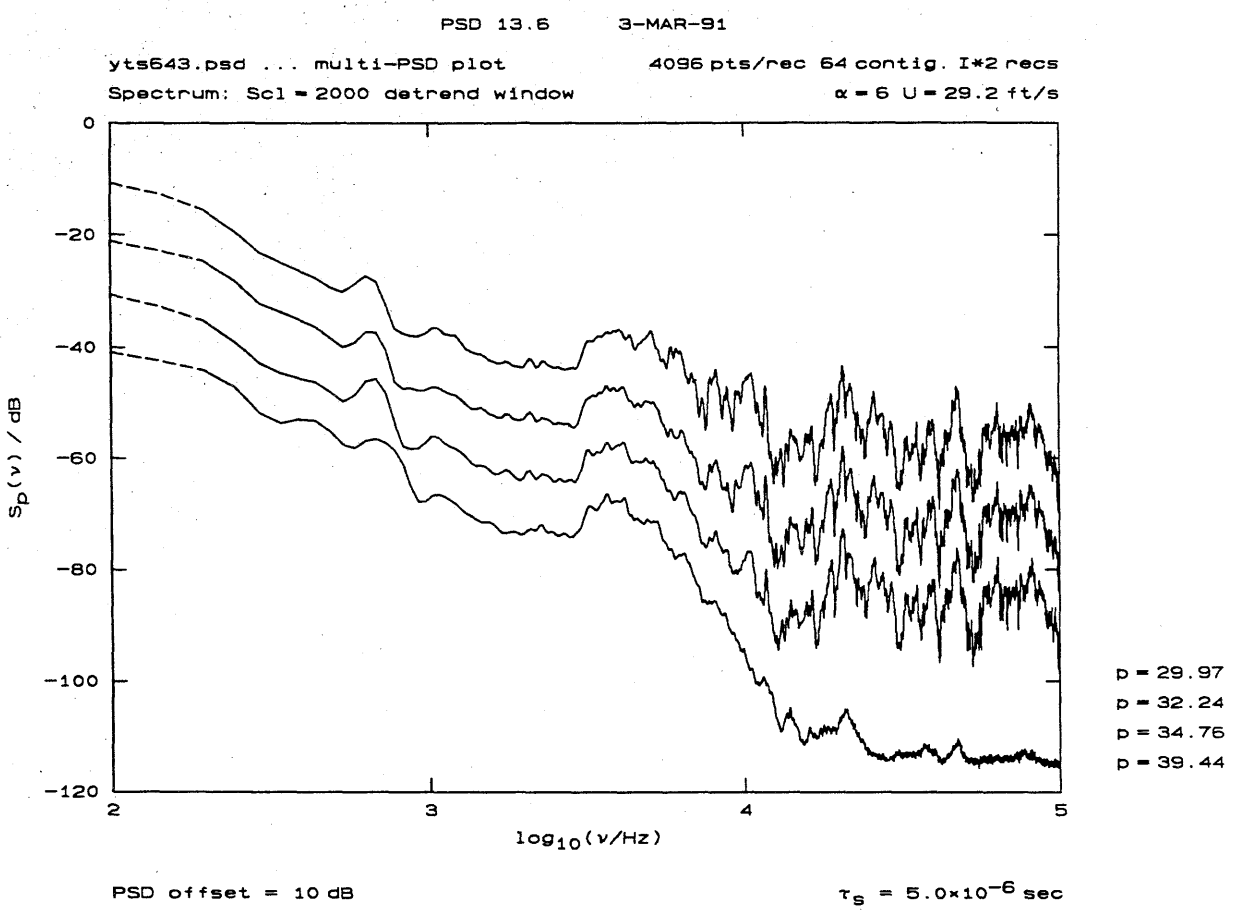

FIG. 24 Hydroacoustic spectra at $\alpha = 6°$ and $U_{\text{test}} = 29.2\,\text{ft/s}$ (Runs 643, 644, 646 and 647). Successive spectra offset by 10 dB. Test section pressure (psia) in figure legend, bottom right.

Figure 24 plots the hydroacoustic spectra recorded with $\alpha = 6°$, $U_{\text{test}} \simeq 29\,\text{ft/s}$ (Runs 643, 644, 646 and 647). Note the lower noise floor in the highest pressure spectrum (Run 643, $p_{\text{test}} = 39.44\,\text{psia}$)†. The very small cavitation signature at the highest pressure is noteworthy‡.

† Note that background noise has not been subtracted.

‡ No other evidence for cavitation was noted at the time.

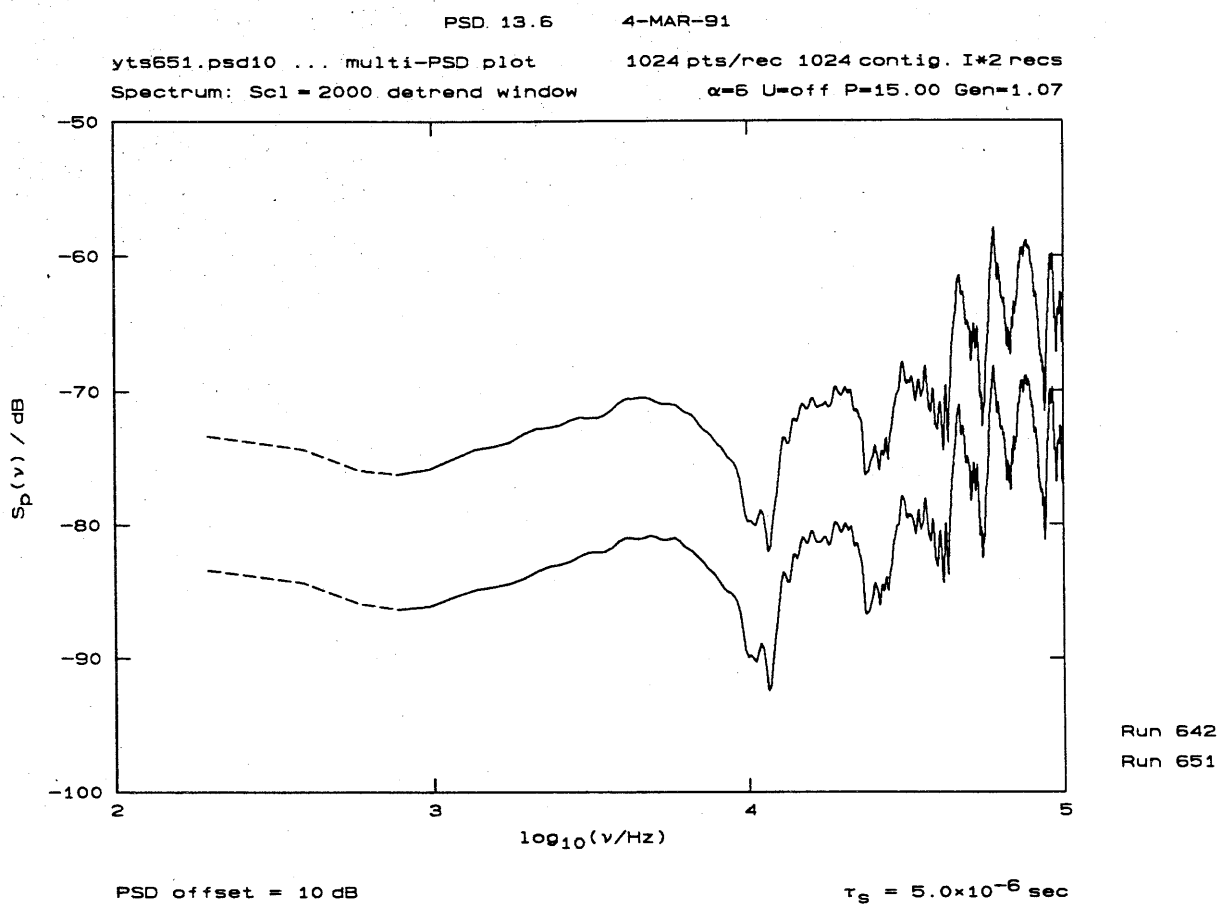

FIG. 25 Comparison of Run 651 and Run 642 acoustic admittance spectra. Hydrofoil at $\alpha = 6°$. The spectra computed from contiguous $2^{10} = 1,024$ point records. Run 642 (top) spectrum offset by 10 dB.

Finally, to check both the reproducibility of the admittance spectrum measurements, as well as assess the statistical confidence of the spectrum estimations, a last pair of runs was performed, repeating the conditions of Runs 641 and 642. The resulting Runs (650 and 651) recorded four times as much data (1,024 records of 1,024 points/record). The two admittance spectra for Runs 642 and 651 are plotted in Fig. 25.

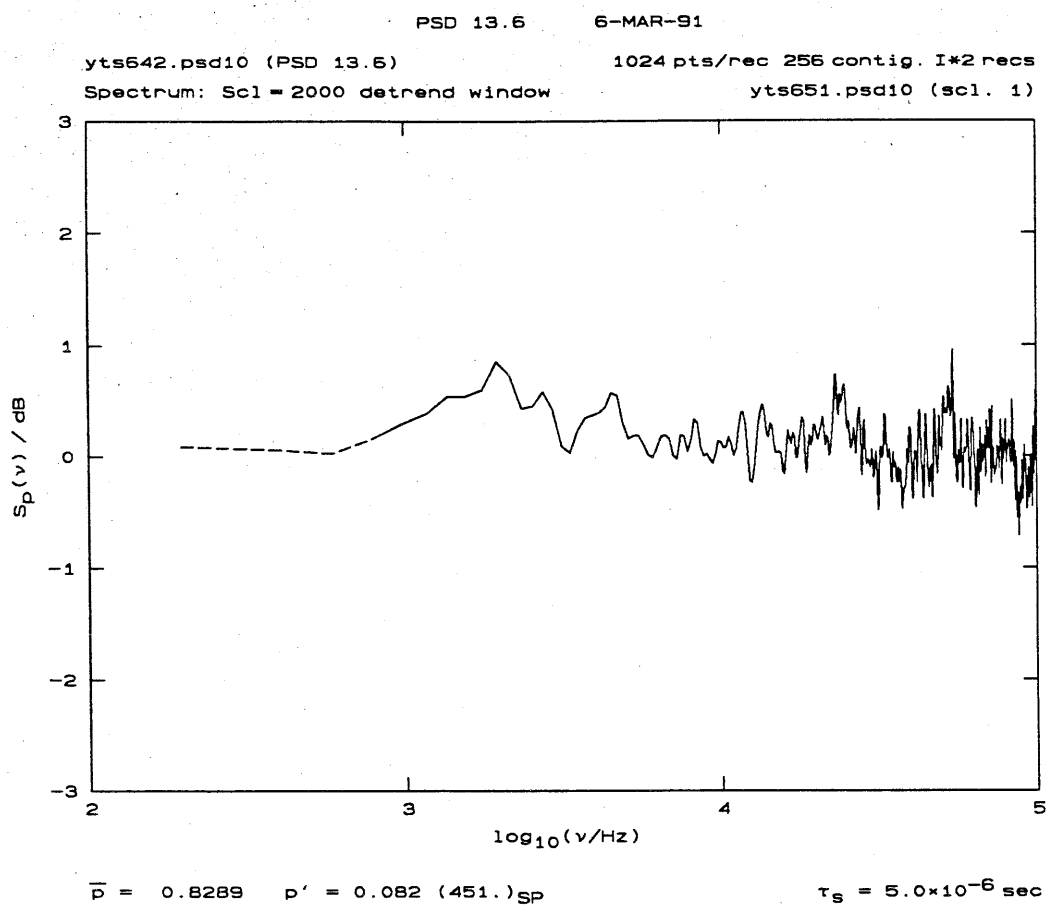

FIG. 26 Comparison of Run 642 and Run 651 acoustic admittance spectra. Plot above is of the quotient [642/651] of the two spectra.

A more direct test is to normalize one spectrum by the other (this can be done by taking the dB-difference of the two). If the two are exactly the same, the normalization should yield 0 dB for the quotient. The result is plotted in Fig. 26. As can be seen, the two are *very* closely matched, down to the fine, high frequency resolution details in the 10 kHz to 100 kHz frequency band. Specifically, the quotient is well within $< \pm 1$ dB of 0 dB, corresponding to an admittance spectrum stability and reproducibility of better than 1%[♯]. We may conclude that the high frequency details are not noise in the spectrum!

We may also conclude that reliable spectrum estimates can indeed be made from the 256 × 1,024 point records that were used throughout this test.

♯ The admittance spectrum has a dynamic range that is greater than 20 dB.

4. The HSWT acoustic environment

It goes without saying that one would prefer, ideally, to conduct hydroacoustic testing in an anechoic environment, typically also in the far field. Considering the range of velocities and frequencies of interest, however, these criteria can typically not be met in conventional testing facilities. As a consequence, it is of paramount important to characterize the acoustic environment of the testing facility so as to be able to correct and compensate for its effects, to the extent possible, so as to best estimate what the acoustic field characteristics *would have been* if the testing could have been conducted in an ideal environment. An exploratory investigation of this possibility was attempted using the measured white noise excitation response of the Tunnel test section acoustic *admittance*. Recall Fig. 10, and related discussion. Those and related results, as well as their potential use, will be discussed below.

At high frequencies, for which the wavelength of sound

$$\lambda = \frac{c}{f} , \tag{1}$$

where $c \simeq 1,500\,\mathrm{m/s}$ is the speed of sound in water and f is the frequency, is comparable or smaller that the test section dimensions, the Tunnel acoustic admittance can be expected to also be a (weak) function of the Tunnel speed. That is because the moving fluid convects the acoustic waves, to some extent, changing the effective dimensions that give rise to acoustic resonances in the Tunnel. More importantly, however, wavelengths in that length range can give rise to resonances with respect to one or more of the Tunnel test section dimensions.

The test section is $h = 30'' = 0.762\,\mathrm{m}$ high, by $b = 6'' = 0.1524\,\mathrm{m}$ across (span) at the hydrofoil midchord station*. As a consequence, we can expect resonances at wavelengths given by

$$\lambda_n = \frac{2\,h}{n} , \qquad n = 1,2,3,\ldots \tag{2a}$$

and

$$\lambda_m = \frac{2\,b}{m} , \qquad m = 1,2,3,\ldots , \tag{2b}$$

corresponding to frequencies

$$f_n = n\frac{c}{2\,h} \simeq 1.0\,n\,\mathrm{kHz} , \qquad n = 1,2,3,\ldots \tag{3a}$$

and

$$f_m = m\frac{c}{2\,b} \simeq 5.0\,m\,\mathrm{kHz} , \qquad m = 1,2,3,\ldots , \tag{3b}$$

---

* The test section span has a slight diverging taper in the downstream direction to offset pressure gradients that would otherwise arise from boundary layer displacement effects.

and lower, owing to the test section divergence in the downstream direction.

Considering the location of the acoustic driver and receiver that were used to estimate the acoustic admittance, we can expect that the f_n resonance family will not be well represented. The f_n modes have nodes on the test section upper and lower flow guidewalls, where the acoustic driver and receiver are located. Evidence that the fundamental, $f_{n=1}$, can be excited by the hydrofoil flow and cavitation noise sources can be seen in the spectra in Fig. 15.

The prominent bulge in the hydroacoustic spectra around $4-5\,\mathrm{kHz}$, *e.g.* Fig. 5, may be attributable to a near-coincidence of the fundamental mode of the f_m resonance family, the fourth mode of the f_n resonance family, as well as, possibly, one of the test section structural modes. It would require the Tunnel admittance to be properly measured, *i.e.* corresponding to the acoustic path from the hydrofoil to the receiving hydrophone, to compensate for the increased admittance corresponding to this path, for that effect to be accounted for.

Direct evidence for the f_m mode family, Eq. 3b, whose fundamental is at $5\,\mathrm{kHz}$, can be seen in the admittance plots in Figs. 10 and 22. We can expect the fundamental, $f_{m=1}$ to be excited by the acoustic driver, but not the next, $f_{m=2}$, mode at $\sim 10\,\mathrm{kHz}$. The latter has a mid-span node, where the acoustic driver and receiver were also located. On the other hand, that mode could be excited by hydrofoil-generated flow or cavitation noise sources, which are distributed across the test section span, even though it is not likely to be well received (low "antenna gain")**. The dip in the admittance spectrum around $f \simeq 10\,\mathrm{kHz}$ (*e.g.* Fig. 23) corroborates this caveat.

The potential utility of the admittance spectrum can be illustrated by using it to compensate for the (here, high) frequency response of the Tunnel, by *normalizing* the measured hydroacoustic spectra by the acoustic admittance†. To increase the statistical significance of this procedure, the hydroacoustic spectra were recomputed as derived from (four times as many) contiguous records, comprised, however, of $2^{10} = 1,024\,\mathrm{points/rec}$ each. The normalized admittance spectrum estimate at $\alpha = 6°$ was plotted in Fig. 23.

** In retrospect, if the acoustic driver and receiver had been slightly offset from the test section midspan axis, they would have been less sensitive to the Tunnel test section acoustic resonance structure.

† The validity of this procedure rests on the assumption that the acoustic processes can be regarded as linear uncoupled responses to the hydrodynamic and cavitation processes. Compensation then amounts to subtraction on the dB-axis.

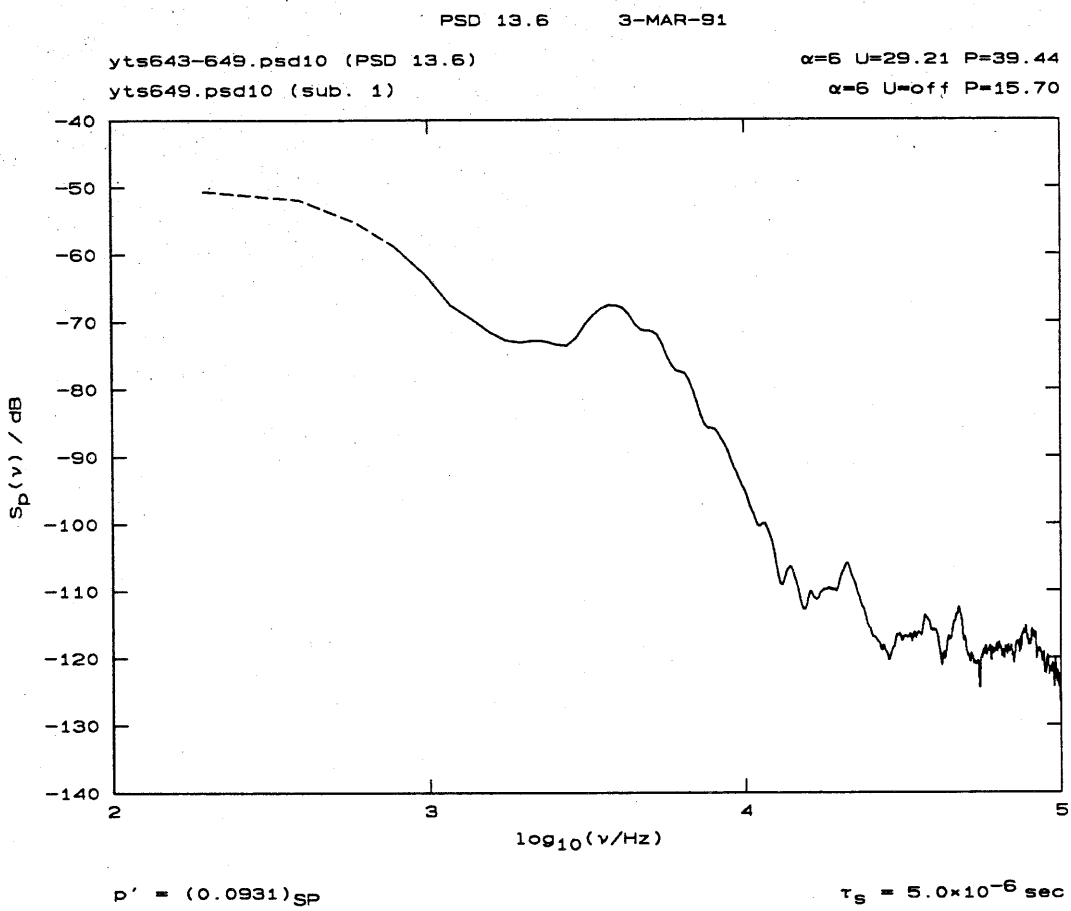

FIG. 27 Hydroacoustic spectrum, measured at $\alpha = 6°$, $U_{\text{test}} \simeq 29.2\,\text{ft/s}$, and $p_{\text{test}} = 34.44\,\text{psia}$ (Run 643; *cf.* Fig. 24), computed for $1,024\,\text{pt/rec}$ data. Background noise (Run 649) spectrum has been subtracted.

The hydroacoustic spectrum for the data measured at $\alpha = 6°$, $U_{\text{test}} \simeq 29.2\,\text{ft/s}$ and $p_{\text{test}} = 34.44$ (Run 643) was similarly computed and the background noise (Run 649) was subtracted. Figure 27 plots the resulting hydroacoustic spectrum estimate. The lower noise figure from the improved signal acquisition, higher amplifier gain, as well as the increased statistical confidence in the individual spectra and, hence, their difference, allows an additional 10 dB improvement in the hydroacoustic spectrum estimate.

This spectrum was then compensated, by normalizing with the admittance spectrum in Fig. 23, as described above. The result is plotted in Fig. 28. The large dynamic range exhibited by this spectrum is not an artifact. The increased Tunnel admittance (and receiver assembly "antenna gain") at high frequencies permits acoustic signals to be detected that would otherwise be much closer to the total electronic and other noise of the total measurement system.

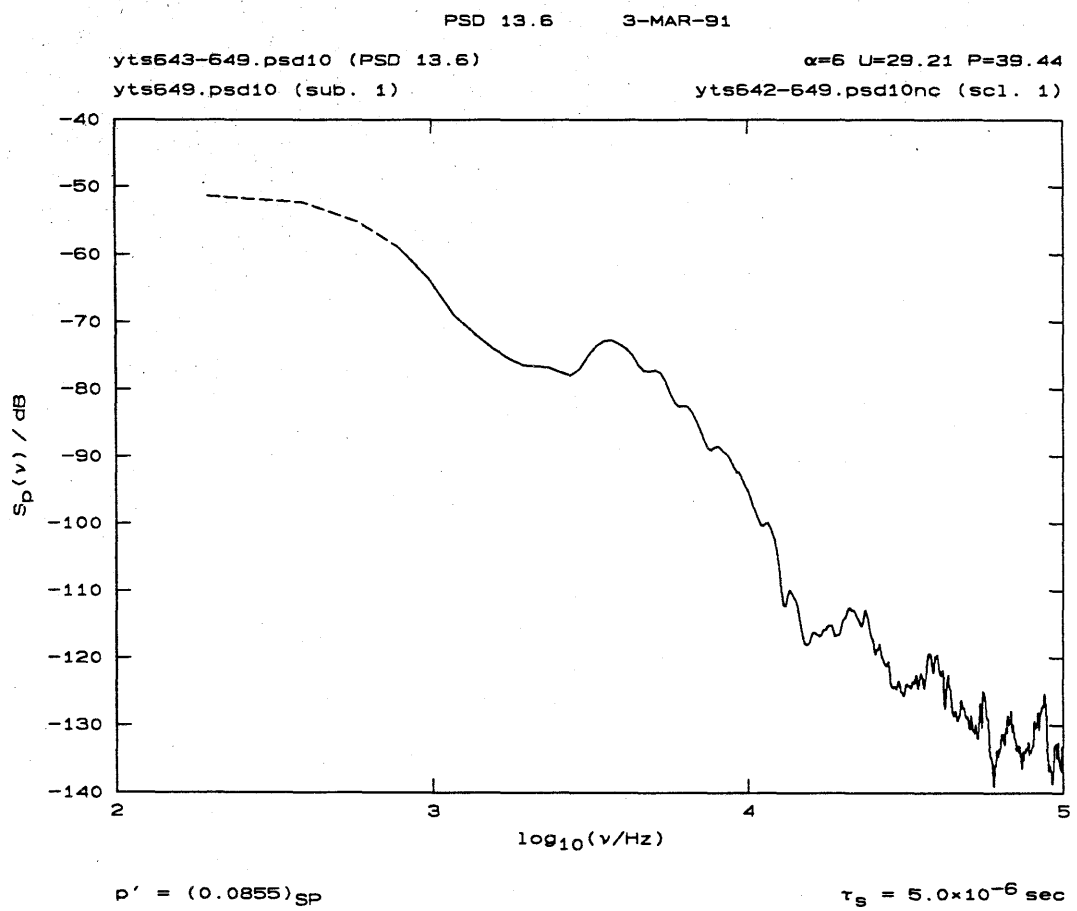

FIG. 28 Hydroacoustic spectrum of Fig. 27, compensated using the admittance spectrum in Fig. 23, to provide a far-field estimate.

The compensated spectrum exhibits a much more uniform roll-off as the acoustic frequency is increased, as expected. The spectrum seems to roll-off with a slope close to $-40\,\mathrm{dB/decade}$, *i.e.* is close to

$$S_p(f) \simeq \text{const.} \times f^{-4} \ , \tag{4}$$

in the frequency range $1\,\mathrm{kHz} \leq f \leq 100\,\mathrm{kHz}$.

Recall that the mid-height location of the hydrofoil and the acoustic sources associated with the flow around it was not the same as the location of the white noise generator (projector) that was used to estimate the Tunnel acoustic admittance†. As a consequence, many of the spectral features that remain are probably attributable to the fact that the acoustic admittance that was used for the compensation does not exactly correspond to the one that should have been applied, as

† The latter was mounted opposite the receiver, on the Tunnel test section bottom guide wall.

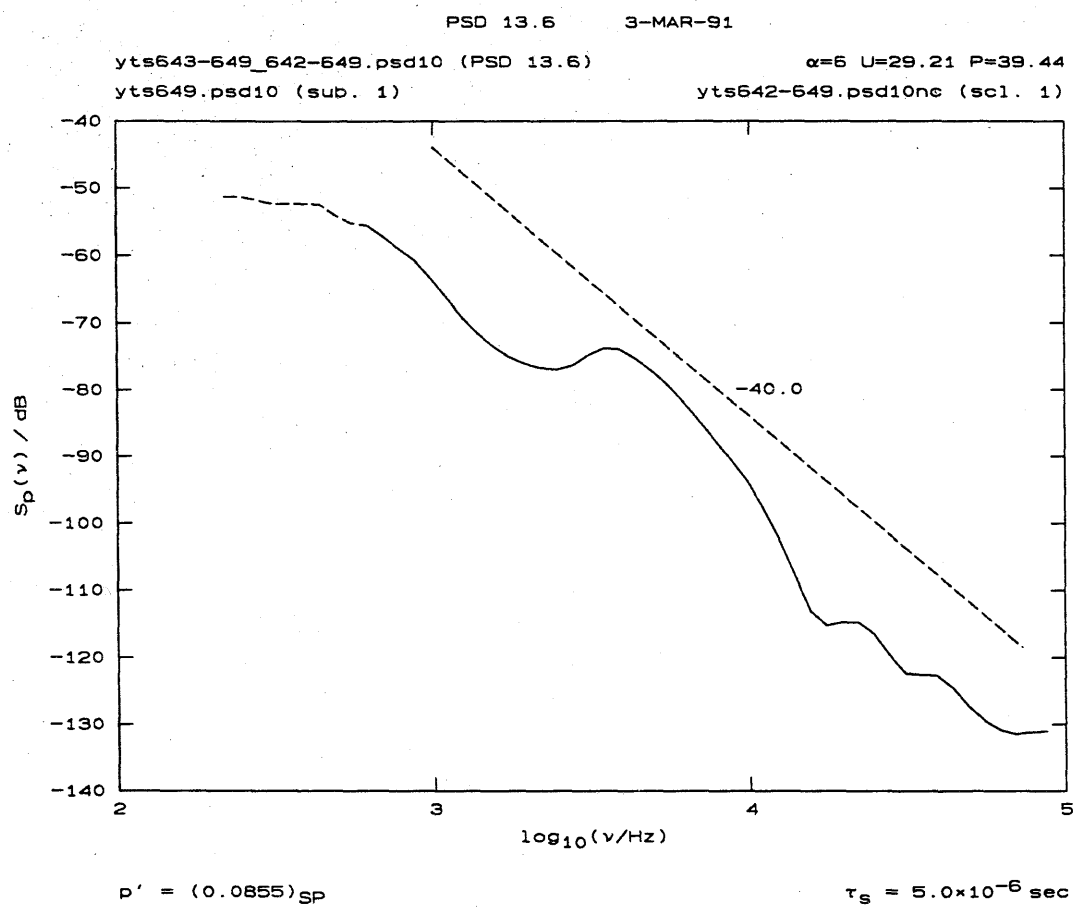

FIG. 29 Hydroacoustic spectrum in Fig. 28, smoothed using a 1/3-octave filter, with a reference slope line at $-40\,\mathrm{dB/decade}$.

noted earlier. In particular, this is likely the case for the large bump in the vicinity of $f \approx 5\,\mathrm{kHz}$.

This spectrum is replotted in Fig. 29, using a 1/3-octave smoothing filter. The latter is the more conventional means of computing and displaying acoustic spectra. Comparing Figs. 29 and 28, however, we see that it masks many features that require higher fractional frequency resolution, *i.e.*

$$\frac{\delta f}{f} < \frac{1}{3}\,\text{octave} \approx \frac{1}{10}\,\text{decade}\ , \tag{5}$$

to be discerned. The two spectra can be compared by holding the two pages against the light. The reference slope line included in Fig. 29 is at $-40\,\mathrm{dB/decade}$.

5. Discussion and conclusions

The primary objectives of this test were met. Specifically, the results have shown that hydroacoustic spectra can be measured to good accuracy in the test environment of the GALCIT High Speed Water Tunnel, over a range of test section speeds and static pressures.

The acoustic receiver/driver assemblies that were developed for this test represents, to the best of my knowledge, an advance in the methods that have been employed to date. The advances in signal and digital data acquisition that we have made at GALCIT in the last decade, or so, have permitted the acoustic spectra to be measured to a very high signal-to-noise ratio, approaching $90 - 95\,\mathrm{dB}$ under certain flow conditions, over a high frequency range, with a high frequency resolution. This allowed the measurement of hydroacoustic spectra at high frequencies, whose power lies many decades below that of the low frequency part of the pressure fluctuation spectrum. It is in this frequency range where the onset of cavitation can best be detected. While these specifications proved adequate for the purposes of this test, it should also be noted that they do not represent the limit of what is possible.

The utility of being able to measure the contribution to the fluctuations at high frequency is illustrated in Fig. 30, where the acoustic pressure fluctuation rms, computed for the frequency band $10\,\mathrm{kHz} \leq f \leq 100\,\mathrm{kHz}$, *i.e.*

$$p' = \left[2 \int_{10\,\mathrm{kHz}}^{100\,\mathrm{kHz}} S_p(f)\, df \right]^{1/2} , \tag{6}$$

is plotted *vs.* the test section pressure. The data were recorded with $\alpha = 2°$ and $U_{\mathrm{test}} \simeq 20\,\mathrm{ft/s}$ (Runs 599–606, *cf.* Fig. 18). Note that the rms plotted represents the sum of the contribution of the electronic and other noise, added on top of the hydroacoustic pressure fluctuation*. The rms acoustic pressure fluctuation is in the same units as the hydroacoustic spectrum in Fig. 18. These data allow the specification of the cavitation onset to be determined, under these flow conditions, to be close to $\log_{10}(p_{\mathrm{test}}/\mathrm{psia}) \simeq 0.65$, or $p_{\mathrm{test}} \simeq 4.5\,\mathrm{psia}$.

The corresponding data were computed from the spectra recorded with $\alpha = 6°$, at $U_{\mathrm{test}} \simeq 30\,\mathrm{ft/s}$ (Runs 630–636, *cf.* Fig. 21). The results are plotted in Fig. 31. As was also evident in the spectra in Fig. 21, the onset of cavitation, under these flow conditions, is much more dramatic and the acoustic power levels generated much higher. As it turns out, under these flow conditions, the onset of cavitation seems to occur very close to a test pressure of Run 632, *i.e.* $p_{\mathrm{test}} \simeq 34.86\,\mathrm{psia}$.

---

* The background noise has not been subtracted.

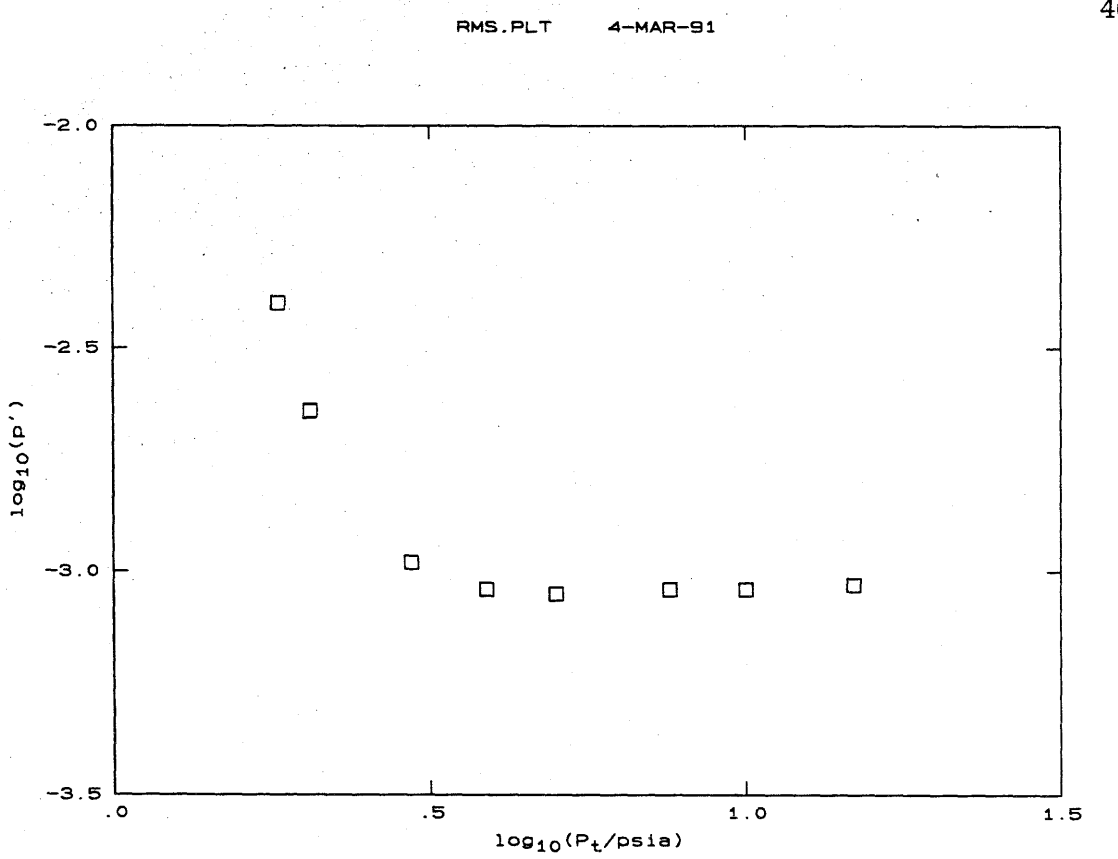

FIG. 30 Acoustic pressure rms in the frequency range $10\,\text{kHz} \leq f \leq 100\,\text{kHz}$, *vs.* test section pressure. Recorded at $\alpha = 2°$ and $U_{\text{test}} \simeq 20\,\text{ft/s}$ (*cf.* Fig. 18). Cavitation onset at $p_{\text{test}} \simeq 4.5\,\text{psia}$ (see text).

As regards cavitation inception, it was possible to conclude, on the basis of these tests, that its onset was always traceable to the root junction formed between the two-dimensional hydrofoil and the Tunnel sidewall(s). The inference is that the strength of the hairpin vortex that wraps around the hydrofoil root junction is such as to produce the lowest static pressures near the leading edge in the vicinity of this junction. As noted earlier, particle paths in the vicinity of the core of this vortex are also characterized by a long residence time, to the extent that they traverse the region in front of the hydrofoil near its stagnation line. That makes such paths particularly important in initiating cavitation inception as they combine the low pressure with the long (Lagrangian) time that is important for bubble growth**.

A method was developed to quantify the testing environment acoustic admittance. The spectrum of this quantity can be used to compensate the hydroacoustic spectrum, to a large extent, for the fact that the measurements were not conducted

** This observation arose out of discussions that I would like to acknowledge with Prof. Stephen Cowley, of Cambridge University, DAMTP, who was visiting Caltech at the time.

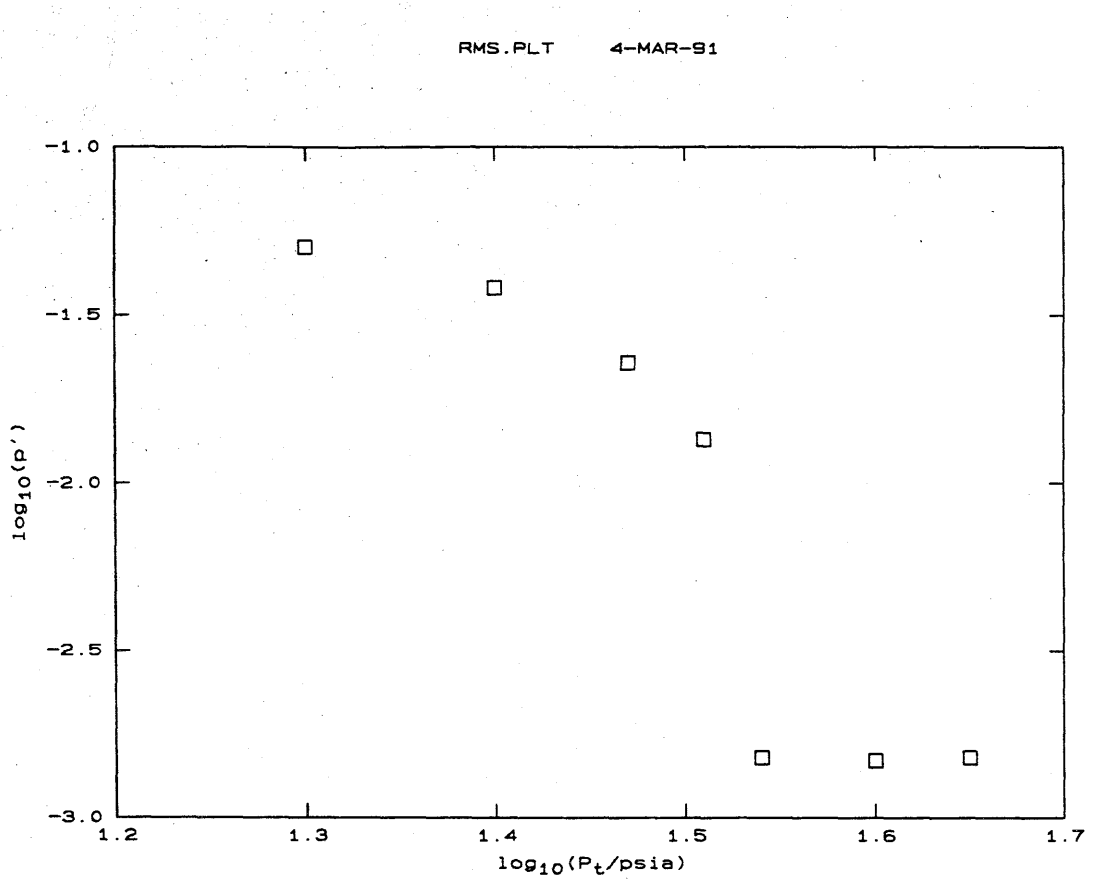

FIG. 31 Acoustic pressure rms in the frequency range $10\,\text{kHz} \leq f \leq 100\,\text{kHz}$, *vs.* test section pressure. Recorded at $\alpha = 6°$ and $U_{\text{test}} \simeq 30\,\text{ft/s}$ (*cf.* Fig. 21). Cavitation onset at $p_{\text{test}} \simeq 34.86\,\text{psia}$.

in an anechoic environment. On the other hand, the feasibility of such a compensation was demonstrated by measuring the acoustic admittance for a convenient path in the HSWT test section that did not represent the best approximation for the acoustic path whose admittance would needs to be calibrated, namely from the hydrofoil to the acoustic receiving transducer assembly. While such an admittance calibration *can* be performed, it would have required the redesign of the large sidewall window of the Tunnel, to permit mounting of the acoustic driver near the location of the hydrofoil. That represented a much larger undertaking than could have been contemplated, given the budgetary constraints that were placed on this effort.

It should be noted, however, that such a modification to the High Speed Water Tunnel *could* be undertaken. If successful, it would permit one to approximate far-field hydroacoustic measurements in an enclosed environment. If such an effort were to be undertaken, one should use the opportunity to also redesign the face of the HSWT 2-D test section sidewall window, as well as the top and bottom test section guidewalls, so as to provide as close to an anechoic environment, at least for the

high frequency members of the f_n resonance family (Eq. 3a) and the f_m resonance family (Eq. 3b), as possible. While a discussion of such a design is beyond the purposes of this report, I believe that it could be realized in a way that would not disturb the flow.

A less expensive improvement could be attempted in the future that would locate the acoustic driver and receiver slightly offset from the Tunnel midspan axis (recall discussion and footnote on p. 41). This would result in a lower coupling between the Tunnel acoustic resonance structure and the acoustic receiver, lowering the dynamic range of the acoustic admittance, and, as a consequence, of the necessary associated compensation to the hydroacoustic spectra.

6. References

BALOGA, P. [1982] "Water Tunnel Tests on NACA–66 (modified) and YS–920 Foil Sections With and Without Surface Roughness", GALCIT HSWT Report No. 1139.

BARKER, S. J. [1974] "Measurements of radiated Noise in the Caltech High-Speed Water Tunnel. Part I: Radiated Noise from Turbulent Boundary Layers", ONR Contract N00014–67–A–0094–0028 (NR 062–462) Report.

BARKER, S. J. [1975] "Measurements of radiated Noise in the Caltech High-Speed Water Tunnel. Part II: Radiated Noise from Cavitating Hydrofoils", ONR Contract N00014–67–A–0094–0028 (NR 062–462) Report.

BARKER, S. J. [1976] "Measurements of hydrodynamic noise from submerged hydrofoils", *J. Acoust. Soc. Am.* **59**(5), 1095-1103.

DIMOTAKIS, P. E., GAEBLER, H. F., HAMAGUCHI, H. T., LANG, D. B. and SHEN, Y. T. [1988] "Two-dimensional NACA 66 (MOD) Hydrofoil High Speed Water Tunnel Tests", GALCIT Report HSWT 1142.

SHEN, Y. T. and DIMOTAKIS, P. E. [1989a] "The Influence of Surface Cavitation on Hydrodynamic Forces", 22^{nd} *American Towing Tank Conference* (St. John, Newfoundland, Canada), August 1989.

SHEN, Y. T. and DIMOTAKIS, P. E. [1989b] "Viscous and Nuclei Effects on Hydrodynamic Loadings and Cavitation of a NACA 66 (MOD) Foil Section", *J. Fluids Eng.* **111**, 306–316.

APPENDIX A
Acoustic transducer calibrations

A.1 Acoustic driver

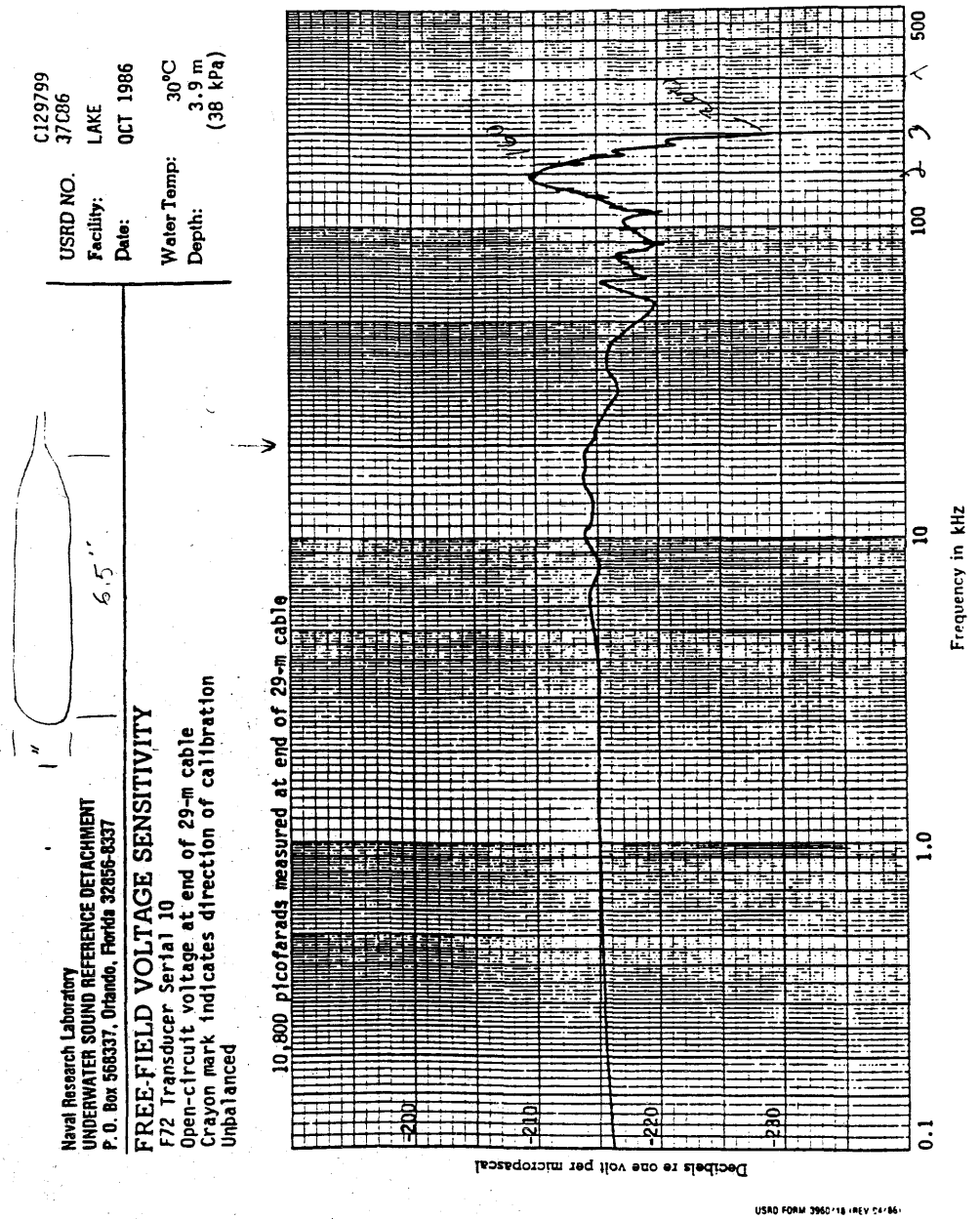

A.2 Acoustic receiver